Design of a 'smart' startup-profile for an Automatic Balancing Unit

Design of a 'smart' Startup-Profile for an Automatic Balancing Unit

R.M.C. Mestrom

Report no. DCT. 2003-23

Research report

Coaches: Prof.dr. H. Nijmeijer
ir. R.A. van Rooij
dr.ir. N. van de Wouw

Eindhoven University of Technology
Department of Mechanical Engineering
Dynamics and Control Group

Eindhoven, May 2003

Abstract

In rotating machines, imbalance is a main engineering problem, as it is a standard cause of vibrations. Balancing of the rotor can be a very time-consuming and delicate operation in the production or design process. Balancing refers to the process of getting rid of imbalance. Several solutions are available for balancing, but which of these solutions is most effective depends on the 'type' of imbalance. Since, in the case of a CD-ROM driveline, as considered in this project, the imbalance is unknown and subject to change, application of an Automatic Balancing Unit (ABU) seems to be an obvious choice.

An ABU consists of a circular disc, concentrically mounted to the rotating machine part, carrying a number of freely moving balls. These balls roll on a dry surface in the rim and, as a result, dry friction effects influence the system performance. In fact, due to stiction, the balls in the ABU do not reach their balancing position (completely), which results in a residual imbalance in the system. As the rotational velocity of the ABU can be prescribed, a 'smart' startup-profile could potentially reduce this residual imbalance by influencing the resulting equilibrium positions.

A dynamic model of an ABU with two balls has previously been derived. In this model, the dry friction between the balls and the rim of the ABU is modeled as Coulomb friction. Here, an extended version of this model is derived. Also the dynamics of the motor driving the ABU are added. Both models have been implemented numerically. By comparing measurements with the latter model, an estimate of the friction coefficient is made, as this parameter highly influences the equilibrium set in which the balls settle.

Based on numerous time simulations with the model without motor behaviour, a startup-profile is designed. Ideal motor control is assumed. During the design process several interesting observations are made with respect to the behaviour of the balls and the equilibrium positions they attain. With the final startup-profile, reproducible ball positions are obtained, resulting in a small residual imbalance together with a small percentage of simulations that result in more imbalance than the system without balls. Finally, the sensitivity of the startup-profile for the friction coefficient is investigated.

This study was performed in the scope of the ADOPT (Sequential Approximate Design Optimization) project. This project aims at developing a new strategy for computer aided optimization of mechanical products, systems and processes exhibiting combinations of uncertainties, discrete design variables and discontinuities. The problem, as formulated in this study, would make an ideal test case for the optimization tool developed in the ADOPT project.

Samenvatting

In roterende machines is onbalans een groot machinebouwkundig probleem , omdat dit een standaard oorzaak van trillingen is. Het balanceren van de rotor kan een erg tijdrovende en fijngevoelige bezigheid zijn in het ontwerpproces. Balanceren duidt op het kwijtraken van de onbalans. Een aantal oplossingen om te balanceren zijn voorhanden, maar welke daarvan het meest effectief is hangt af van het 'type' van de onbalans. Omdat, in het geval van een aandrijflijn van een CD-ROM, die in dit project wordt beschouwd, de de grootte en positie van de onbalans onbekend en veranderlijk zijn, lijkt de toepassing van een Automatic Balancing Unit (ABU) een voor de hand liggende keuze.

Een ABU bestaat uit een cirkelvormige schijf met opstaande rand, die concentrisch is gemonteerd op een roterend machine-onderdeel en een aantal vrij bewegende kogels bevat. Deze kogels rollen over een droog oppervlak in de rand en derhalve beïnvloeden droge wrijvingseffecten de prestatie van het systeem. In feite bereiken de kogels in de ABU, vanwege het stiction-gedrag, niet (geheel) hun balancerende positie, hetgeen resulteert in een rest-onbalans in het systeem. Omdat de rotatiesnelheid van de ABU kan worden voorgeschreven, kan een 'slim' opstartprofiel deze onbalans mogelijk verminderen door de evenwichtsposities te beïnvloeden.

Eerder is er een dynamisch model van de ABU met twee kogels afgeleid. In dit model is de droge wrijving tussen de kogels en de rand van de ABU gemodelleerd als Coulombse wrijving. Hier wordt een uitgebreide versie van dit model afgeleid. Ook is de dynamica van de motor die de ABU aandrijft toegevoegd. Beide modellen zijn numeriek geïmplementeerd. Door het vergelijken van metingen met het laatstgenoemde model, is een schatting van de wrijvingscoëfficiënt gemaakt, aangezien deze parameter grote invloed heeft op de evenwichtsgebieden waarin de kogels uiteindelijk tot rust komen.

Gebaseerd op een groot aantal tijdsimulaties met het model zonder motorgedrag is het opstartprofiel ontworpen. Een ideale motorregeling is hierbij aangenomen. Gedurende het ontwerpproces zijn er enkele interessante waarnemingen gedaan met betrekking tot het gedrag van de kogels en de evenwichtsposities die ze aannemen. Met het uiteindelijke opstartprofiel zijn reproduceerbare posities van de kogels verkregen, hetgeen resulteert in een kleine rest-onbalans, samen met een klein percentage van de simulaties dat resulteert in meer onbalans dan het systeem zonder kogels. Tenslotte is de gevoeligheid van het opstartprofiel onderzocht voor de wrijvingscoëfficiënt.

Deze studie is uitgevoerd in het kader van het ADOPT (Sequential Approximate Design Optimization) project. Dit project streeft naar de ontwikkeling van een strategie voor computerondersteunde optimalisatie van mechanische producten, systemen en processen, die door combinaties van onzekerheden, discrete ontwerpvariabelen en discontinuïteiten gekenmerkt worden. Het probleem zoals geformuleerd in deze studie zou een ideaal testprobleem zijn voor het optimalisatiegereedschap dat in het ADOPT project ontwikkeld wordt.

Contents

Chapter 1

Introduction

In rotating machines, imbalance is a main engineering problem, as it is a standard cause of vibrations. Balancing of the rotor can be a very time-consuming and delicate operation in the production or design process. Balancing refers to the process of getting rid of imbalance. Several solutions are available for balancing, but which of these solutions is most effective depends on the 'type' of imbalance. Since, in the case of a CD-ROM driveline, as considered in this project, the imbalance is unknown and subject to change, application of an *Automatic Balancing Unit (ABU)* seems to be an obvious choice. Therefore, the working principle of the ABU will be explained first. Next, the problem formulation and the motivation for this project will be stated. Finally, an outline for the rest of the report is given.

1.1 Working Principle of the ABU

An Automatic Balancing Unit is a system that is able to counteract imbalance in rotating machines. The system mainly consists of a circular disc with upright rim, concentrically mounted to the rotating machine part, with a number of freely moving balls in it, see figure 1.1. For a rotational frequency of the machine, that exceeds the so-called critical speed of the system, the balls automatically move to a configuration that leads to balancing. The critical speed is the natural frequency of the system. In this way, the imbalance of the system is compensated, and the rotor remains balanced regardless of imbalance variations (within a certain bound). This automatic balancing behaviour will be explained by investigating the working principle of the ABU.

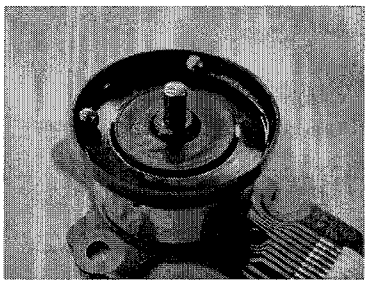

Figure 1.1: Picture of the ABU without CD.

This working principle can be explained using figure 1.2, in which schematic representations of the ABU with two balls are shown. In this representation, the geometrical center of the ABU and the rotor axis are situated in point B. Point mass C represents the imbalance and m_1 and m_2 represent the balls. The resulting imbalance – the resultant of the imbalances of point mass C

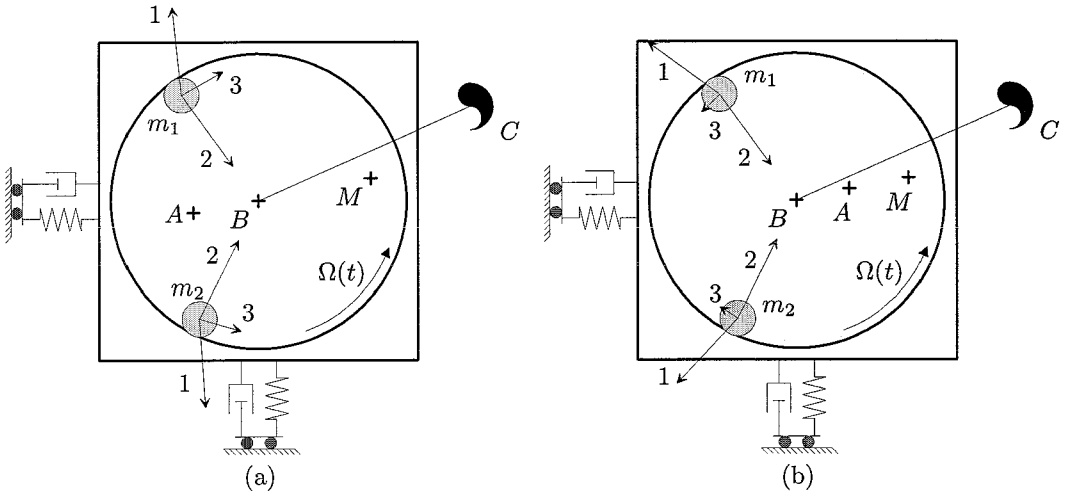

Figure 1.2: Interplay of forces below (a) and above (b) critical speed.

and the balls – is located in point M. When the balls are not moving with respect to the disc and the rotor has a constant rotational speed ($\Omega(t) = \text{constant}$), point B makes a circular orbit with frequency $\Omega(t)$ around point A, which is fixed to the inertial space. Several forces are acting on each ball. First, each ball experiences a centrifugal force (1), which is directed along the line from A to m_i ($i = 1, 2$). Secondly, a normal force (2) is exerted on each ball, directed perpendicular to the rim of the ABU, that is in direction from m_i to B. The resultant force of these two forces is the driving force (3), which acts in tangential direction.

Below the critical speed, which is the natural frequency of the isotropically suspended system, the rotor is in phase with the imbalance, that is, vector $\vec{r}_{AB}$ and vector $\vec{r}_{BM}$ are pointing in the same direction. Above the critical speed, however, these vectors are pointing in opposite directions, which means that the vectors are 180° out of phase. The working principle of the ABU can be understood by reconstructing the interplay of forces belonging to these two situations. In figure 1.2(a), it can be seen that the driving force below the critical speed directs the balls *towards* the imbalance, thus enlarging it. Above the critical speed (figure 1.2(b)), the driving force directs the balls *away from* the imbalance, thereby reducing the imbalance. Finally, when the system is completely balanced, the point A, B and M coincide and the driving force vanishes as the normal and centrifugal force exactly compensate each other.

To balance the system, the balls have to find appropriate equilibrium positions relative to the ABU. This can only take place when a certain dissipative force is present to eventually stop the relative motion of the balls with respect to the ABU. Often, this dissipative effect is provided by means of viscous damping, using oil or some other viscous fluid in the ABU. The Automatic Balancing Unit used for this project is provided by Philips Optical Storage and is used as balancing unit in CD-ROM players. Considering this application, no viscous fluid can be used to dissipate the kinetic energy of the balls as such fluid could destroy the optical system in case of leakage. Instead, the dissipative force is caused by the fact that the balls run on the dry surface of the rim of the ABU and are, therefore, subject to dry friction. The so-called stiction behaviour of this dry friction influences the system dynamics. A first model that describes the ABU with two balls using a 'smooth' friction model is presented in [Koe01]. A second model includes a set-valued Coulomb friction model and is introduced in [Heu02]. In practical applications, the balancing unit can carry up to nine freely moving balls, but for the purpose of simplification and gaining insight in the dynamics this number is reduced to two balls in this project.

1.2 Problem Formulation and Motivation for the Project

Due to the stiction behaviour of dry friction the balls in the ABU do not reach their balancing position (completely), which results in a residual imbalance in the system. This is a major drawback of an ABU with dry friction, as the equilibrium set in which the balls can settle is quite large. In a previous study (see [Heu02]), interesting observations are made about how the resulting equilibrium positions can be influenced. The size of the equilibrium set namely varies with rotational speed and is smallest around the critical speed of the ABU (this will be treated in depth in chapter 4). As the rotational velocity of the ABU can be prescribed, a 'smart' startup-profile could possibly make use of this property of the system, thereby influencing the resulting equilibrium positions. The reproducibility of these equilibrium positions could then be enlarged, resulting in minimal residual imbalance. Therefore, the following problem definition is formulated for this project:

> *Design a 'smart' startup-profile for an Automatic Balancing Unit with two balls, such that reproducible equilibrium positions are obtained and the residual imbalance is reduced.*

Implicitly, this problem definition contains an optimization problem formulation. Therefore, solving this problem involves optimization. From an optimization point of view the ABU problem shows several interesting characteristics. First, the Coulomb friction in the ABU has a discontinuous character. Furthermore, the size and direction of the imbalance of the CD-ROM is an uncertain variable, as well as for example the starting position of the balls. Moreover, the number of balls in the ABU can be seen as a discrete design variable. The ABU, therefore, makes an ideal test case for the optimization tool that is currently being developed in the Dynamics and Control (D&C) Group of the Department of Mechanical Engineering at Eindhoven University of Technology. This optimization tool is developed in the ADOPT (Sequential Approximate Design Optimization) research project. This project aims at developing new strategies for computer aided design optimization of mechanical products, systems and processes exhibiting combinations of uncertainties, discrete design variables and discontinuities.

1.3 Outline of the Report

To obtain a solution to the problem stated in the problem definition, the behaviour of the ABU is analyzed with help of a dynamic model of the ABU as well as measurements at the experimental setup. First, this experimental setup (provided by Philips Optical Storage) is discussed in chapter 2.

Secondly, a time-variant dynamic model of the ABU is presented and the necessity of augmenting it with the dynamic behaviour of the motor driving the ABU is discussed in chapter 3. Moreover, the numerical implementation of this model in MATLAB is illuminated.

Chapter 4 discusses the startup-profile and the choices that are made during its design. Moreover, general demands on the startup-profile and criteria by which it is designed are posed. Subsequently, the steps taken in the design are discussed together with some interesting observations made during the simulations. Next, a final startup-profile is proposed and its sensitivity to the friction parameter is investigated. The chapter ends with an optimization problem layout that could possibly be used as a testcase for the optimization tool as developed in the ADOPT project.

Finally, conclusions are drawn and some recommendations for future research are made in chapter 5.

Chapter 2

Experimental Setup

In this chapter, a description of the experimental setup, as provided by Philips Optical Storage, is given. This setup has been used to perform experiments. Next, the variables that can be measured using the setup are discussed

2.1 Setup Description

In figure 2.1, a picture of the total experimental setup is shown. The same setup was used in the previous study (see [Heu02]). In this setup, the ABU is rigidly attached to the CD. Normally, the ABU would be mounted on top of the CD, but as the balls would not be visible in that case, the CD is mounted *beneath* the ABU. The CD and the ABU are both mounted to the motor. The stator part of this motor is mounted to an aluminum table. This table is supported by 4 steel wits. The spring stiffness of the suspension of the table can be varied by adjusting the length of the wits. Furthermore, an aluminum rod is attached to the table, which is dipped in oil, thus providing for necessary damping in the suspension. The damping level can be varied by varying the length of the part of the rod that is submerged in the oil by varying the oil level or by varying the viscosity of the oil.

To reduce the influence of external factors, this total setup is placed on top of a granite block of large mass (110 kg), which is placed on a separate table. The isolation of the experimental setup from its surroundings is established and is shown to be sufficient in [Heu02].

The CD with imbalance, which is used in the experiments, consists of an ordinary CD with 24 equidistant holes drilled in it in a concentrical pattern. The imbalance in the CD is provided by putting small screws in several of the holes (the CD without screws is carefully balanced beforehand).

Moreover, some remarks have to be made about the motor driving the ABU. It can operate at a wide range of angular velocities, varying from approximately -5 to -255 Hz (-31.4 to -1602.2 rad/s). The value of the rotational velocity is negative because the motor turns clockwise, whereas the counterclockwise direction will be defined as positive in section 3.1.3. The motor velocity is controlled by a steering unit on a printed circuit board which is in turn operated by a PC. The controller that controls the motor velocity has several parameters that can be adjusted in the steering program. Furthermore, it is possible to prescribe a rotational velocity profile in the steering program, which the motor control will follow as well as possible. One problem arising here, however, is that the steering program can only have trajectories prescribed with a resolution in angular velocity of 1 Hz. More on this topic will be discussed in section 3.2.3. A final remark on the motor control has to be made: the angular velocity realized by the motor shows a slight mismatch with the target frequency given in the steering program. A reason for this could not be found, but the behaviour is examined experimentally and the following approximate linear

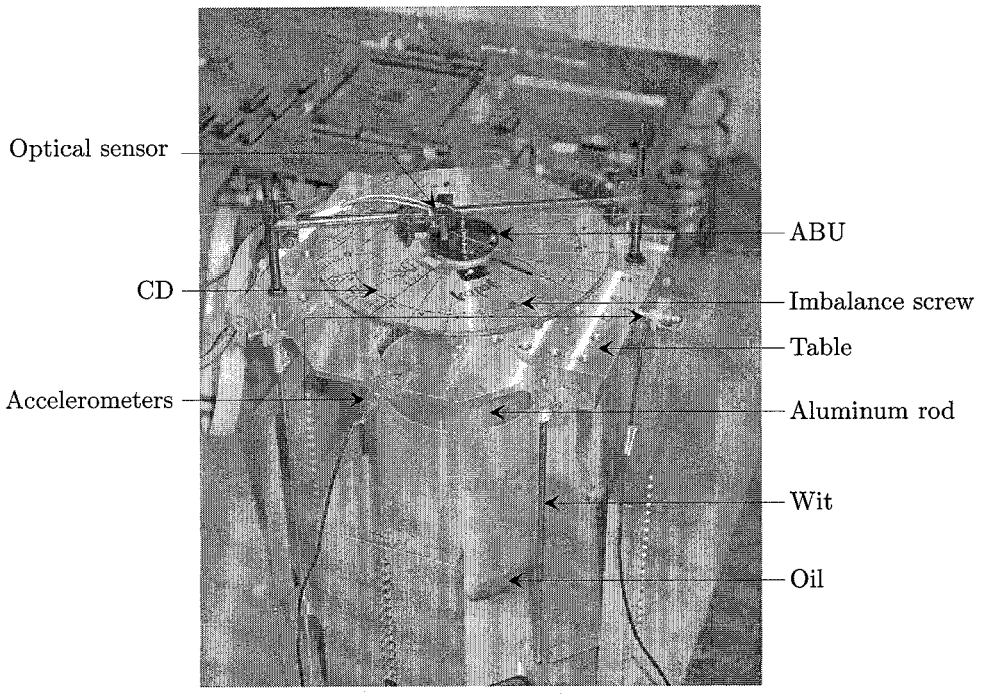

Figure 2.1: Picture of the experimental setup.

dependency between the 'real' frequency and the target frequency is found (see equation (2.1)):

$$f_{real} = f_{target} - \frac{f_{target} + 1}{64}. \tag{2.1}$$

This means that at a target frequency of 63 Hz the 'real' frequency is 1 Hz lower (in equation (2.1) the frequency needs to be positive for validity of the equation).

The balls used in the experiment are made of brass. Other balls could also be used but are subject to magnetic forces, thereby attracting or repelling each other and influencing the behaviour in an undesired manner. The brass balls do not suffer from this effect.

Finally, there are some cleaning restrictions to the measurements. Before each series of measurements, the balls and the polycarbonate ABU are thoroughly cleaned with an isopropanol tissue. Care must be taken that after cleaning, squeezers are used to put the balls in the ABU again as the friction contact between the balls and the rim of the ABU changes due to pollution.

2.2 Measured Variables

In the experimental setup, several variables can be measured. First, the movement of the table is measured by means of two accelerometers, providing information on the linear acceleration of the table in two directions, see figure 2.1.

Furthermore, the positions β_i $(i = 1, 2)$ of the balls can be measured by two different methods. The first method uses an optical sensor mounted to the aluminum table (see figure 2.1). The sensor, being rigidly fixed to this table, is aligned above the rim of the ABU and registers the passings of each ball by means of light reflection. Moreover, a steel wire, which is also detected by the optical sensor, is spanned over the ABU (see figure 2.2). The wire acts as a static reference, meaning that the wire does not move relative to the imbalance of the CD. The measurement signal from the optical sensor consists of a stationary signal with 'peaks' in it, according to the steel wire and ball passings. By comparing the occurrence of the peaks related to the balls, with the peaks

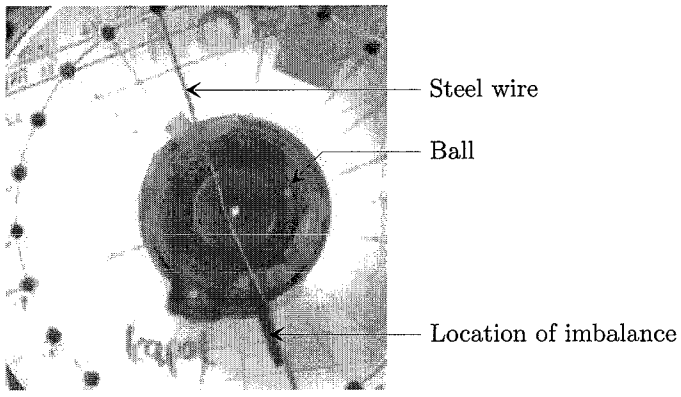

Figure 2.2: Top view of the ABU with CD (only one ball is depicted).

related to the wire, it is possible to determine the ball angles in the ABU with respect to the imbalance position. (The ball angle at the side of the imbalance is defined to be 0 [rad].) Passings of the steel wire include a small and large gap in between two successive peaks respectively, which is caused by the fact that the wire is not spanned exactly over the geometrical center of the ABU (see figure 2.2). Moreover, one half of the wire is slightly thicker than the other half, thus giving larger peaks. The accuracy with which the angular position of the balls can be determined, depends strongly on the frequency at which the data from the optical sensor is sampled and the rotational frequency of the ABU. By monitoring the angular position of the balls during time, an indication of the transient behaviour of the balls can be obtained.

The second technique for the ball position measurement uses a high speed camera, placed above the ABU setup (the optical sensor is removed). With help of picture analysis software, the transient ball positions can be measured. However, because of the very limited amount of time the camera can measure (approximately 0.68 s at 4500 Hz) and the extensive amount of time that is taken by data transport from the camera to the analysis computer, this method is not used. Furthermore, a sufficiently accurate estimate of the ball positions for the purpose of this research can easily be obtained using the first method.

An example of a measurement using the first method can be found in appendix A. Moreover, the analysis of this measurement is explained here, together with the interpolation algorithm written in MATLAB for this purpose.

Chapter 3

Modeling the ABU and the Motor

This chapter discusses the construction of a dynamic model of the ABU, using Lagrange's equations for systems with constraints. In section 3.2, the derivation of the equations of motion of the motor is presented as well as the expansion of the dynamic model of the ABU with these terms. Moreover, the numerical implementation of the model is discussed briefly in section 3.3, which is concluded with the description of the final simulation model.

3.1 The Dynamic Model of the ABU

3.1.1 Model Definition

A schematic representation of the ABU can be seen in figure 3.1. One of the underlying assumptions of this representation, is that all movements of the ABU-system take place in the horizontal plane. The 4 wits with which the ABU is suspended are modeled as two linear springs k_1 and k_2.

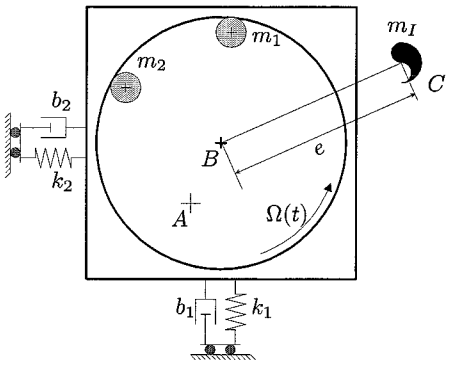

Figure 3.1: Schematic model of the ABU.

Displacements are assumed to be small enough for these springs to be considered linear. Moreover, the damping of the rod dipped in the oil is represented by two linear dampers b_1 and b_2. In this approach it is assumed that the table only makes translational movements and does not rotate.

The ABU is rigidly attached to the motor. This motor is rigidly attached to the table. The total mass of the table, motor, CD (without imbalance) and the ABU (without balls) equals M_T. The imbalance is located on the CD in point C at distance e from the geometrical center of the ABU (point B). Furthermore, the ABU contains two freely moving balls of mass m_i $(i = 1, 2)$, subject to friction forces acting in tangential direction. These balls are assumed to be permanently in contact with the rim of the ABU, under influence of centrifugal forces. Moreover, in the model

it is assumed that the balls cannot contact each other, which means that no impact model has to be used.

Point A is considered to be the origin of the inertial space. For a perfectly balanced system or a system at rest, points A and B coincide. When the system is not balanced, point B describes a motion around point A.

3.1.2 Kinematics of the ABU Model

In order to be able to derive a dynamic model of the ABU system, first the kinematics and the coordinates used to describe the kinematics have to be elucidated. Figure 3.2 shows a schematic kinematic model of the ABU. In figure 3.2, the inertial coordinate system $(\vec{e}_1, \vec{e}_2)$ is located in

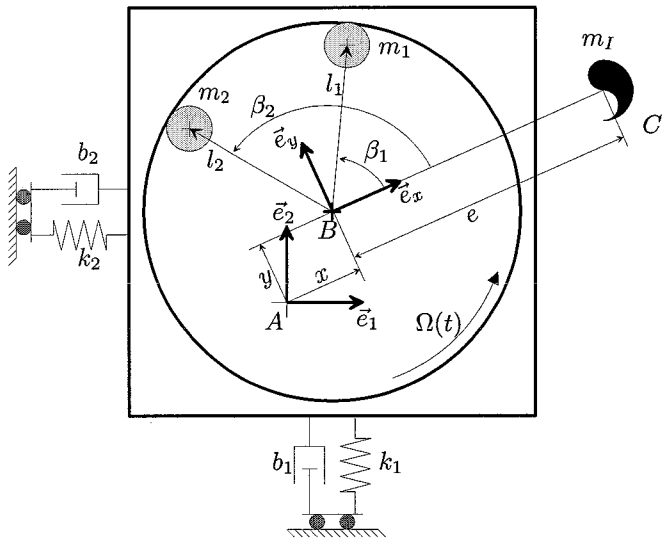

Figure 3.2: Kinematic model of the ABU.

point A, whereas the body-fixed coordinate system $(\vec{e}_x, \vec{e}_y)$ is located in point B. The rotation imposed to the ABU and CD by the motor is given by $\Omega(t)$ and is directed in counter-clockwise direction. In the body-fixed coordinate system the imbalance can be described by a constant vector $\vec{r}_{BC} = e\vec{e}_x$. Point B describes a motion with frequency $\Omega(t)$ around point A and its position with respect to point A is described by the two coordinates x and y in coordinate system $(\vec{e}_x, \vec{e}_y)$. Otherwise, these two coordinates would be rotation dependent, which would not be a sensible choice. Furthermore, the positions of the balls can be described using β_i and l_i $(i = 1, 2)$, relative to coordinate system $(\vec{e}_x, \vec{e}_y)$.

By the introduction of the angle $\theta(t) = \int_0^t \Omega(\tau)d\tau + \theta(0)$ and defining $\theta(0) = 0$, the relationship between the two coordinate systems can be described by using direction cosine matrix $\underline{A}^{10}$:

$$\begin{bmatrix} \vec{e}_x \\ \vec{e}_y \end{bmatrix} = \underline{A}^{10} \begin{bmatrix} \vec{e}_1 \\ \vec{e}_2 \end{bmatrix} = \begin{bmatrix} \cos\theta(t) & \sin\theta(t) \\ -\sin\theta(t) & \cos\theta(t) \end{bmatrix} \begin{bmatrix} \vec{e}_1 \\ \vec{e}_2 \end{bmatrix}. \tag{3.1}$$

The position vectors needed to derive the dynamic model are given by:

$$\vec{r}_{AB} = \begin{bmatrix} x & y \end{bmatrix} \begin{bmatrix} \vec{e}_x \\ \vec{e}_y \end{bmatrix}, \tag{3.2}$$

$$\vec{r}_{AC} = \vec{r}_{AB} + e\,\vec{e}_x, \tag{3.3}$$

$$\vec{r}_{Am_i} = \vec{r}_{AB} + \begin{bmatrix} l_i\cos\beta_i & l_i\sin\beta_i \end{bmatrix} \begin{bmatrix} \vec{e}_x \\ \vec{e}_y \end{bmatrix}, \; i = 1, 2. \tag{3.4}$$

Therefore, the kinematics of the system can be described using six generalized coordinates: x, y, β_1, β_2, l_1 and l_2.

3.1.3 Derivation of the Dynamic Model

The dynamic model of the ABU has been derived using Lagrange's method for systems with constraints (see for example [Wou02]). The complete derivation can be found in appendix B and is almost equal to the one followed in [Heu02]. Some explanatory remarks have to be made however. In the derivation, it is assumed that the friction present between the balls and the rim of the ABU can properly be described by the Coulomb friction model. This model states that:

$$f_w \in \mu f_n \text{Sign}(\dot{\beta}), \tag{3.5}$$

where $\text{Sign}(\beta)$ denotes the set-valued sign-function:

$$\text{Sign}(\dot{\beta}) = \begin{cases} 1 & \dot{\beta} > 0 \\ [-1,1] & \dot{\beta} = 0 \\ -1 & \dot{\beta} < 0 \end{cases}. \tag{3.6}$$

The parameters f_w, f_n and μ can be found in table 3.1.

Furthermore, to avoid numerical problems and to reduce the number of parameters, the equations of motion are written in a non-dimensional form, in which the time scale is stretched. In order to do this, the following non-dimensional parameters and coordinates are introduced:

$$\bar{x} = \frac{x}{L}, \quad \bar{l}_1 = \frac{l_1}{L}, \quad \bar{d}_1 = \frac{d_1}{L}, \quad \bar{m}_1 = \frac{m_1}{M}, \quad \bar{J}_1 = \frac{J_1}{m_1 d_1^2} = \frac{1}{10},$$
$$\bar{y} = \frac{y}{L}, \quad \bar{l}_2 = \frac{l_2}{L}, \quad \bar{d}_2 = \frac{d_2}{L}, \quad \bar{m}_2 = \frac{m_2}{M}, \quad \bar{J}_2 = \frac{J_2}{m_2 d_2^2} = \frac{1}{10},$$
$$\bar{\Omega} = \frac{\Omega}{\omega_n}, \quad \bar{e} = \frac{e}{L}, \quad \bar{m}_I = \frac{m_I}{M}, \quad \bar{b} = \frac{b}{2M\omega_n},$$

where $M = M_T + m_I + m_1 + m_2$ and $\omega_n = \sqrt{\frac{k}{M}}$. The variables and parameters can be found in table 3.1.

Table 3.1: Explanation of the symbols and parameters used in the dynamic model.

x	Displacement in $\vec{e}_x$-direction [m]	μ	Friction coefficient [-]
y	Displacement in $\vec{e}_y$-direction [m]	J_i	(Polar) Moment of inertia of ball around center of gravity i [kg m^2]
β_i	Angle of ball i with respect to $(\vec{e}_x, \vec{e}_y)$	M_T	Total mass of the table, motor, ABU (without balls) and CD (without imbalance) [kg]
l_i	Distance from B to center of ball i [m]	M	Total mass of the system [kg]
L	Distance from B to center of the balls (L has a constant value) [m]	k	Spring stiffness [N/m]
e	Distance from B to imbalance [m]	b	Damping coefficient [Ns/m]
d_i	Diameter of ball i [m]	t	Time [s]
m_I	Mass of imbalance [kg]	Ω	Driving angular velocity [rad/s]
m_i	Mass of ball i [kg]	ω_n	Eigenfrequency of the system [rad/s]
f_w	Coulomb friction force [N]		
f_n	Normal force [N]		

Furthermore, a non-dimensional time-scale is introduced: $\bar{t} = \omega_n t$. Consequently, derivatives with respect to this time-scale can be defined:

$$(\dot{\cdot}) = \frac{d(\cdot)}{d\bar{t}} = \frac{1}{\omega_n}\frac{d(\cdot)}{dt} \text{ and } (\ddot{\cdot}) = \frac{d^2(\cdot)}{d\bar{t}^2} = \frac{1}{\omega_n^2}\frac{d^2(\cdot)}{dt^2}.$$

Moreover, non-dimensional versions of the normal (f_{n_i}) and friction forces (f_{w_i}) have to be derived:

$$\bar{f}_{n_i} = \frac{f_{n_i}}{m_i\omega_n^2 L}, \text{ and } \bar{f}_{w_i} = \frac{f_{w_i}}{m_i\omega_n^2 L}.$$

Finally, the column of non-dimensional generalized coordinates ($\underline{q}$) can be defined as $\underline{q} = \begin{bmatrix}\bar{x} & \bar{y} & \beta_1 & \beta_2 & \bar{l}_1 & \bar{l}_2\end{bmatrix}^T$. The parameters and symbols introduced, are explained in table 3.1. An isotropic suspension of the table is assumed, which means that $k_1 = k_2 = k$ and $b_1 = b_2 = b$.

With these definitions, Lagrange's equations for systems with constraints can be used, which leads to the following general form of the equations of motion (see appendix B):

$$\underline{M}(\underline{q})\ddot{\underline{q}} + \underline{H}(\underline{q},\dot{\underline{q}}) + \underline{S}\,\underline{\lambda} \ni \underline{R}^T\underline{\lambda}, \tag{3.7}$$

where the non-dimensional mass-matrix is given by:

$$\underline{M}(\underline{q}) = \begin{bmatrix} 1 & 0 & -\bar{m}_1\sin\beta_1 & -\bar{m}_2\sin\beta_2 & \bar{m}_1\cos\beta_1 & \bar{m}_2\cos\beta_2 \\ 0 & 1 & \bar{m}_1\cos\beta_1 & \bar{m}_2\cos\beta_2 & \bar{m}_1\sin\beta_1 & \bar{m}_2\sin\beta_2 \\ -\sin\beta_1 & \cos\beta_1 & 1+4\bar{J}_1 & 0 & 0 & 0 \\ -\sin\beta_2 & \cos\beta_2 & 0 & 1+4\bar{J}_2 & 0 & 0 \\ \cos\beta_1 & \sin\beta_1 & 0 & 0 & 1 & 0 \\ \cos\beta_2 & \sin\beta_2 & 0 & 0 & 0 & 1 \end{bmatrix}, \tag{3.8}$$

and

$$\underline{H}(\underline{q},\dot{\underline{q}}) = -\left[h_{\bar{x}} \quad h_{\bar{y}} \quad h_{\beta_1} \quad h_{\beta_2} \quad h_{\bar{l}_1} \quad h_{\bar{l}_2}\right]^T, \text{ with:} \tag{3.9}$$

$$\begin{aligned}
h_{\bar{x}} &= -2\dot{\bar{y}}\bar{\Omega} - \bar{x}\bar{\Omega}^2 - \bar{m}_I\bar{e}\bar{\Omega}^2 - \dot{\bar{\Omega}}(\bar{y} + \bar{m}_1\sin\beta_1 + \bar{m}_2\sin\beta_2) \\
&\quad -\bar{m}_1(\dot{\beta}_1+\bar{\Omega})^2\cos\beta_1 - \bar{m}_2(\dot{\beta}_2+\bar{\Omega})^2\cos\beta_2 + \bar{x} + 2\bar{b}(\dot{\bar{x}} - \bar{y}\bar{\Omega}), \\
h_{\bar{y}} &= 2\dot{\bar{x}}\bar{\Omega} - \bar{y}\bar{\Omega}^2 + \dot{\bar{\Omega}}(\bar{x} + \bar{m}_I\bar{e} + \bar{m}_1\cos\beta_1 + \bar{m}_2\cos\beta_2) \\
&\quad -\bar{m}_1(\dot{\beta}_1+\bar{\Omega})^2\sin\beta_1 - \bar{m}_2(\dot{\beta}_2+\bar{\Omega})^2\sin\beta_2 + \bar{y} + 2\bar{b}(\dot{\bar{y}} + \bar{x}\bar{\Omega}), \\
h_{\beta_1} &= 2\dot{\bar{x}}\bar{\Omega}\cos\beta_1 + 2\dot{\bar{y}}\bar{\Omega}\sin\beta_1 + \bar{x}\bar{\Omega}^2\sin\beta_1 - \bar{y}\bar{\Omega}^2\cos\beta_1 \\
&\quad +\dot{\bar{\Omega}}(\bar{x}\cos\beta_1 + \bar{y}\sin\beta_1 + 1 - 2\bar{d}_1\bar{J}_1), \\
h_{\beta_2} &= 2\dot{\bar{x}}\bar{\Omega}\cos\beta_2 + 2\dot{\bar{y}}\bar{\Omega}\sin\beta_2 + \bar{x}\bar{\Omega}^2\sin\beta_2 - \bar{y}\bar{\Omega}^2\cos\beta_2 \\
&\quad +\dot{\bar{\Omega}}(\bar{x}\cos\beta_2 + \bar{y}\sin\beta_2 + 1 - 2\bar{d}_2\bar{J}_2), \\
h_{\bar{l}_1} &= 2\dot{\bar{x}}\bar{\Omega}\sin\beta_1 - 2\dot{\bar{y}}\bar{\Omega}\cos\beta_1 - \bar{x}\bar{\Omega}^2\cos\beta_1 - \bar{y}\bar{\Omega}^2\sin\beta_1 \\
&\quad -(\dot{\beta}_1+\bar{\Omega})^2 + 2\bar{J}_1\dot{\beta}_1(\bar{d}_1\bar{\Omega} - 2\dot{\beta}_1) + \dot{\bar{\Omega}}(\bar{x}\sin\beta_1 - \bar{y}\cos\beta_1), \\
h_{\bar{l}_2} &= 2\dot{\bar{x}}\bar{\Omega}\sin\beta_2 - 2\dot{\bar{y}}\bar{\Omega}\cos\beta_2 - \bar{x}\bar{\Omega}^2\cos\beta_2 - \bar{y}\bar{\Omega}^2\sin\beta_2 \\
&\quad -(\dot{\beta}_2+\bar{\Omega})^2 + 2\bar{J}_2\dot{\beta}_2(\bar{d}_2\bar{\Omega} - 2\dot{\beta}_2) + \dot{\bar{\Omega}}(\bar{x}\sin\beta_2 - \bar{y}\cos\beta_2).
\end{aligned}$$

The matrix $\underline{R}$ is given by

$$\underline{R} = \begin{bmatrix} 0 & 0 & 0 & 0 & -1 & 0 \\ 0 & 0 & 0 & 0 & 0 & -1 \end{bmatrix}, \tag{3.10}$$

the matrix $\underline{S}$ corresponding to the friction forces equals

$$\underline{S} = \begin{bmatrix} 0 & 0 \\ 0 & 0 \\ \mu_1\text{Sign}(\dot{\beta}_1) & 0 \\ 0 & \mu_2\text{Sign}(\dot{\beta}_2) \\ 0 & 0 \\ 0 & 0 \end{bmatrix} \tag{3.11}$$

and the constraint forces are given by:

$$\underline{\lambda} = \begin{bmatrix} \bar{f}_{n,1} \\ \bar{f}_{n,2} \end{bmatrix}. \tag{3.12}$$

The constraint equations are written on acceleration level, namely as $\underline{R}\ddot{\underline{q}} = \underline{0}$.

The equations derived in this way equal those derived in [Heu02], but contain additional terms with $\dot{\bar{\Omega}}$ to describe the time-variant behaviour of the ABU, necessary for the startup-profile.

3.1.4 Parameter Identification

For the parameter values that are required in the equations of motion, the same values are taken as derived in previous research (see [Heu02]). For the sake of completeness, these values are given in table 3.2. Note that the two balls in the system are identical ($m_1 = m_2$ and $d_1 = d_2$). Furthermore,

Table 3.2: Parameter values for the ABU model.

Parameter	Value	
M_T	$3.24 \cdot 10^{-1}$	[kg]
b	1.28	[Ns/m]
k	$1.07 \cdot 10^{4}$	[N/m]
L	$1.15 \cdot 10^{-2}$	[m]
m_1	$1.4 \cdot 10^{-4}$	[kg]
m_2	$1.4 \cdot 10^{-4}$	[kg]
d_1	$3.0 \cdot 10^{-3}$	[m]
d_2	$3.0 \cdot 10^{-3}$	[m]
m_I	$5.6 \cdot 10^{-4}$	[kg]
e	$3.7 \cdot 10^{-3}$	[m]
μ	$2.75 \cdot 10^{-3}$	[-]

the size and position of the imbalance in the CD is adjustable, however for this study only one imbalance value is considered. With these parameter values the natural frequency of the system becomes $\omega_n = \sqrt{\frac{k}{M}} = 182$ rad/s or 28.9 Hz.

In the previous study (see [Heu02]), the value of the friction coefficient was not determined in a straightforward way. In section 4.2 it will be discussed that strong indications arise that the friction coefficient is larger than the value given in table 3.2. More recent experiments confirm these indications (see [Suy03]).

3.2 The Dynamic Model of the Motor

3.2.1 Derivation of the Motor Model

In order to design a suitable startup-profile for the ABU system, the dynamic behaviour of the motor driving the system is modeled as well. This is done because of the overshoot in the angular velocity that is observed after specifying a frequency setpoint to the control unit (see figure A.2).

The relevant motor behaviour is described with a second-order differential equation. From the documentation file belonging to the motor control (see [Phi02]), it is known that the angular velocity controller is a PI-controller (proportional and integral control action) on the angular velocity. The derivation of the equations of motion for the motor control is given in appendix C. The following differential equation results:

$$J[\ddot{\vartheta} - 2\xi\omega_m(\dot{\vartheta}_{ref} - \dot{\vartheta}) - \omega_m^2(\vartheta_{ref} - \vartheta)] = T_b + \sum_{i=1}^{2} f_{w_i} l_i, \tag{3.13}$$

with ϑ the absolute angle of the disc in radians, ω_m the natural frequency of the motor system in rad/s and ξ the non-dimensional damping coefficient. Furthermore, T_b is the friction couple acting on the motor (for example friction in the bearings) and a force due to the friction between ball i and the rim is present on radius l_i ($i = 1, 2$). The latter term will be discussed in section 3.3.2 in more detail.

3.2.2 Parameter Identification

For the identification of the parameters of the motor controller, experiments have been conducted in which a angular velocity setpoint is prescribed to the motor control. From the extracted responses, a qualitative estimate of the relevant parameters can be made. The aim is to merely obtain a qualitative estimate, as it is not the goal of this study to model the motor as accurate as possible. The experiments have been carried out without balls, thus the term with f_{w_i} $(i = 1, 2)$ in equation (3.13) can be omitted. Experiments were performed for a range of setpoint frequencies: from 10 to 28 Hz in steps of 2 Hz. From these experiments, it is noted that the response is *not* reproducible for setpoint frequencies of 22 Hz and above (this will be addressed in the next paragraph). The estimation of the parameters is, therefore, performed for setpoint frequencies below 22 Hz. In figure 3.3, a qualitative fit of a model response to a measured response is

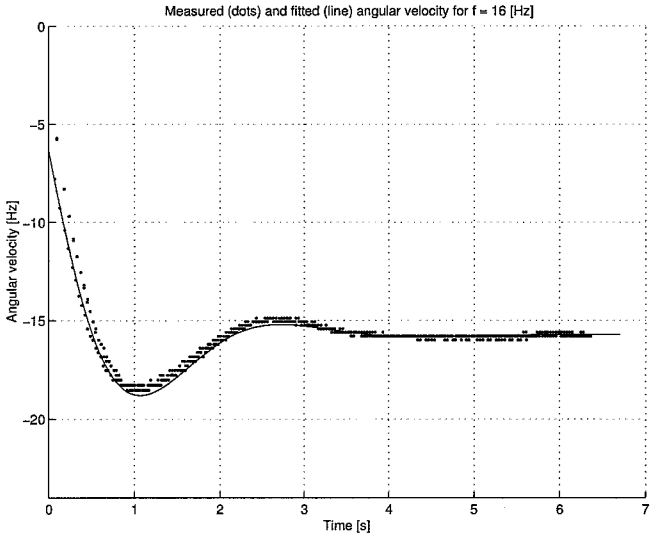

Figure 3.3: Three measured angular velocity step responses (dots) and the fitted response (line).

depicted. For each series of experiments, that is, for each setpoint frequency below 22 Hz, a similar fit is made. The parameters that give an overall best fit for all the measurement series are given in table 3.3. The model seems to capture the relevant behaviour quite accurately. It should be mentioned, however, that due to the interpolation algorithm (see appendix A), the measured response shows a timing mismatch with the fitted one. This is caused by buffering in the data acquisition interface, thus causing the measurement *not* to start at time $t = 0$ s, but later. (However, in the data-file and the interpolation algorithm, the response is stored however as if it has started at $t = 0$ s.) A solution to this is found by shifting the fitted response back in time, thus obtaining the estimates as can be found in table 3.3. The parameter J is found from [Phi02].

Table 3.3: Parameter values for the motor model.

Parameter	Value	
ω_m	0.7π	[rad/s]
ξ	0.5	[-]
T_b	$5.0 \cdot 10^{-4}$	[Nm]
J	$30 \cdot 10^{-6}$	[kg m^2]

3.2.3 Non-Reproducibility in the Experimental Setup

As was mentioned in section 3.2.2, the responses of the motor control are non-reproducible in the neighbourhood of the natural frequency of the ABU system ($f_n = 28.9$ Hz) and above. Figure 3.4 illustrates this non-reproducibility. An explanation for this effect is not found, but a possible cause is the natural frequency of the ABU system, acting as an (additional) disturbance on the motor system. In this figure, a series of 10 experiments is depicted in which a setpoint of 24 Hz is prescribed.

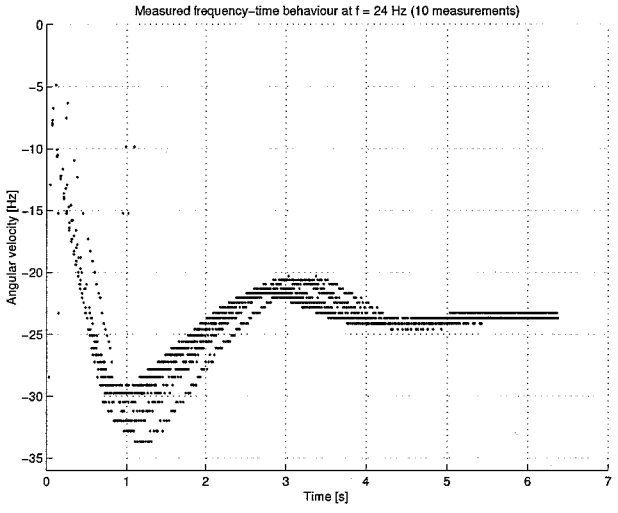

Figure 3.4: Measured rotational frequency responses to setpoint of $f = 24$ Hz.

It should be noted that there are some faulty points in the measured frequency, which can be attributed to the interpolation algorithm, but nevertheless it can be concluded that the motor behaviour is very non-reproducible. After observing this behaviour, an effort is made to prescribe some kind of reference trajectory to the motor control unit, but without succes. Prescribing for example an inclined sine function (to be discussed in section 4.1.3), does not result in the desired behaviour as sometimes even larger overshoots result, compared to the case in which a setpoint is provided. Describing such a function to increase the angular velocity from 10 to 20 Hz in 5 seconds even resulted first in a decrease in angular velocity! Partly, these phenomena stem from the fact that the steering program demands for the setpoint to be given in discrete 1 Hz steps; so smooth functions have to be discretized and cannot be handled properly. Unfortunately, no satisfying solution has been found for this during the project.

3.3 Numerical Implementation

The equations of motion of both the ABU system and the ABU system with the motor control have been implemented in the software package MATLAB. For this purpose, the equations of motion and the constraint equations on acceleration level are combined to obtain expressions for the constraint forces and the accelerations, explicitly.

3.3.1 Implementation of the ABU Model

The equations of motion of the ABU system and the constraint equations are given as:

$$\underline{M}(\underline{q})\ddot{\underline{q}} + \underline{H}(\underline{q}, \dot{\underline{q}}) + \underline{S}\,\underline{\lambda} \ni \underline{R}^T\underline{\lambda}, \tag{3.14}$$

$$\underline{R}\ddot{\underline{q}} = \underline{0}. \tag{3.15}$$

Expressions for the constraint forces and accelerations are found from combining equations (3.14) and (3.15):

$$\underline{\lambda} \in \left[\underline{R}\,\underline{M}(\underline{q})^{-1}(\underline{R}^T - \underline{S})\right]^{-1} \underline{R}\,\underline{M}(\underline{q})^{-1}\underline{H}(\underline{q},\dot{\underline{q}}), \tag{3.16}$$

$$\begin{aligned}\ddot{\underline{q}} &\in -\underline{M}(\underline{q})^{-1}\left[\underline{H}(\underline{q},\dot{\underline{q}}) - (\underline{R}^T - \underline{S})\underline{\lambda}\right] \\ &\in -\underline{M}(\underline{q})^{-1}\left[\underline{I} - (\underline{R}^T - \underline{S})[\underline{R}\,\underline{M}(\underline{q})^{-1}(\underline{R}^T - \underline{S})]^{-1}\underline{R}\,\underline{M}(\underline{q})^{-1}\right]\underline{H}(\underline{q},\dot{\underline{q}}),\end{aligned} \tag{3.17}$$

where $\underline{I}$ is the (6×6) identity matrix.

In this way a system of Ordinary Differential Equations (ODE) is obtained, which is to be solved in MATLAB using an ODE-solver. Furthermore, the system has to be rewritten in state space. Moreover, because the constraints are formulated on acceleration level, constraint stabilization has to be ensured. This is done by explicitly setting $\ddot{l}_i = 0$ $(i = 1, 2)$ each integration step. Although this is *no* guarantee that constraint stabilization is achieved, the method proves to be sufficient for this system. Finally, to overcome numerical problems because of the discontinuous term $\text{Sign}(\dot{\beta}_i)$ a so-called switch-model is implemented as an approximation of the vector field around the surface $\dot{\beta}_1 = \dot{\beta}_2 = 0$. More information on the switch-model can be found in [Lei00]. As an ODE-solver, the ODE23S-algorithm is used for time integration as it yields quick and accurate results.

3.3.2 Implementation of the ABU Model with the Motor

The system of state space equations, obtained in the previous paragraph can be extended with motor equation (3.13). For this purpose the motor equation is made non-dimensional similar to the approach followed in section 3.1.3 for the ABU model. Implementation takes place in the same way as in equations (3.16) and (3.17), with the difference that the column $\underline{q}$ is expanded with the rotational coordinate ϑ.

Furthermore, this additional equation contains terms with the friction forces f_{w_i}, and thus the normal or constraint forces. By adding the equation it is, therefore, no longer possible to derive a closed form expression for the constraint forces as the angular acceleration $\dot{\Omega}$ $(= \ddot{\vartheta})$ is needed in $\underline{H}(\underline{q},\dot{\underline{q}})$ (see equation (3.9)). Because $\ddot{\vartheta}$ is *not* a state (only ϑ and $\dot{\vartheta}$ are), it both depends on the constraint forces and is used to compute these forces. Moreover, it is not sure whether the contribution of these friction forces is significant.

To investigate this, an extended ODE-file is constructed in which the angular acceleration $\ddot{\vartheta}$ $(= \dot{\Omega})$ is refined in an iterative way. This means that in the first iteration the friction forces in (3.13) are omitted and that the constraint forces and the accelerations are calculated using the extended versions of (3.16) and (3.17). Successive iterations calculate an updated $\ddot{\vartheta}$, using the friction forces computed from the constraint forces from the previous iteration. Monitoring the value of $\ddot{\vartheta}$ during several iterations, showed that the friction forces do not contribute significantly and, therefore, they are omitted in further calculations.

3.3.3 Final Simulation Models

Using the models describing the ABU and the motor in the previous sections, two simulation models can be distinguished, both of which will be used in the process of designing the startup-profile in chapter 4. For sake of brevity, the two models will be referred to as follows: the term *ABU-model* will be used to denote the dynamic model of the ABU without the motor behaviour and the term *total ABU-model* will be used for the model with motor behaviour. Note that in both models a startup-profile can be prescribed. In the ABU-model this is done by prescribing Ω and $\dot{\Omega}$ as functions of time and in the total ABU-model the functions ϑ_{ref} and $\dot{\vartheta}_{ref}$ are to be prescribed. The two models are considered equal if it is assumed that the motor control is 'ideal', meaning that all sorts of reference trajectories would be tracked without error. However, this is not the case, which is the reason for the distinction between the two modeling methods.

Chapter 4

Design of the Startup-Profile

In this chapter, the design process of the startup-profile is discussed. First, the general idea behind the startup-profile is explained. Next, in section 4.2 an estimate for the friction coefficient is proposed, which differs significantly from the value used until now. Furthermore, the general choice of startup-profile is discussed. The final startup-profile will consist of two parts. In section 4.3, the first part of the profile is designed, which aims at obtaining reproducible ball positions. Next, the second part of the profile, an increase of the angular velocity to the target frequency, is discussed in section 4.4. Moreover, the sensitivity of the startup profile to the friction parameter is investigated (section 4.5). The chapter is concluded with an optimization problem layout to perform an optimization on the ABU system.

4.1 General Idea and Design Criteria

As stated in section 1.2, it was observed in a previous study (see [Heu02]) that the size of the equilibrium set varies as a function of the rotational frequency and is smallest around the critical speed of the ABU system. This equilibrium set consists in fact of equilibrium *points* of the system around which *areas* arise because of the dry friction behaviour of the ABU (a more in-depth discussion of this can be found in [Heu02]). The general idea behind the startup-profile is that by cleverly making use of the frequency dependency of the equilibrium set, one can influence the resulting equilibrium ball positions. As the only method to have influence on the ABU system is by prescribing the rotational frequency, this method is in fact a kind of manual optimization problem or an open loop control problem.

4.1.1 Design Criteria

Furthermore, as stated in the problem definition, the startup-profile should aim at obtaining reproducible ball positions and reducing the residual imbalance. Before explaining these two goals any further, first, the imbalance of the system *without* balls should be quantified. This imbalance follows from the numerical values in table 3.2:

$$I = m_I e = 2.072 \cdot 10^{-6} \text{ kg m}. \tag{4.1}$$

Reduction of the imbalance is achieved if the balls attain positions for which the total resulting imbalance (related to both the balls and the imbalance in the CD) is less than the value given in equation (4.1). This residual imbalance is calculated from

$$I_r = I + \sum_{i=1}^{2} m_i l_i \cos\beta_i = m_I e + \sum_{i=1}^{2} m_i l_i \cos\beta_i. \tag{4.2}$$

Obtaining reproducible ball positions is a more difficult criterion to explain. The positions are considered reproducible if the resulting ball positions are 'close' together, starting from arbitrary initial conditions. Stated otherwise, this could mean that when a small percentage of the measurements/simulations results in a residual imbalance larger than the the imbalance without balls (see equation (4.1)) this criterion is satisfied. In fact, this is a combination of the demands mentioned above.

Furthermore, a target frequency for the startup-profile has to be specified. Present CD-ROM players reach high angular velocities (up to 200 Hz). However, due to of safety restrictions regarding the forces on the CD-ROM in the experimental setup, the aim is to design a startup-profile that speeds up to $f_{target} = 100$ Hz[1]. The way in which the system realizes this target frequency fully depends on the design of the profile to be discussed in the next sections.

Furthermore, it is known that the ABU system exhibits limit cycling behaviour (see [Heu02]). Limit cycles should however be avoided as their behaviour is highly undesired, because the fact that the residual imbalance will then vary in time.

Other design criteria that could be considered are the following. Because of damage to the playing mechanism or the CD itself, it could be necessary for the vibrational amplitude of the system to stay below a certain value. However, as no information about such an upper bound is present, this criterion is omitted. Moreover, time restrictions to the startup-profile could be given, to define an upper bound to the duration of the transient behaviour. As the problem considered involves an ABU with only *two* balls, the problem is more or less academic. Therefore, it is assumed that there are no time restrictions for the startup-profile (staying within reasonable bounds of for example several minutes). In real applications an ABU would normally contain nine or more balls, which is a totally different situation.

4.1.2 General Assumptions

Since the design of the startup-profile consists of a kind of manual optimization, it is not possible to evaluate the responses of the ABU system to a great diversity of startup-profiles. Therefore, only one kind of startup-profile is used, namely an inclined sine function, which will be be discussed in section 4.1.3. As soon as the optimization tool from the ADOPT project is available, other kinds of startup-profiles can be tested.

Furthermore, for the startup-profile, it is assumed that the system cannot start from arbitrary initial conditions in the 8D-initial condition space $[\bar{x}(0), \bar{y}(0), \beta_1(0), \beta_2(0), \dot{\bar{x}}(0), \dot{\bar{y}}(0), \dot{\beta}_1(0), \dot{\beta}_2(0)]$, but that the system starts at rest. This means that only $\beta_1(0)$ and $\beta_2(0)$ can take arbitrary values between 0 and 2π radians.

As a final assumption, the dynamics of the motor driving the ABU are considered to be less important in the design of the startup-profile. Namely, the motor control in the experimental setup is shown to be non-reproducible (see section 3.2.3) and the steering program cannot handle smooth trajectories. Therefore, the *ABU-model* is used, hereby assuming that the system has an ideal motor with an ideal controller. In future experiments, a different (better) motor and controller could be used to obtain this ideal behaviour. However, the main disadvantage of this assumption is that the startup-profile cannot be tested on the experimental setup.

4.1.3 The Inclined Sine Function

The inclined sine function, which will be used for the design of the startup-profile, is essentially a smooth approximation of a time-function that increases linearly in time to a certain value. The smoothness consists of zero starting and ending slopes of the profile. Namely, the inclined sine function contains no jumps in its first and second time derivative, which is beneficial for smooth control. Therefore, an ideal controller of the motor system could easily follow this angular velocity trajectory. The equation of the inclined sine function (Ω) and its derivative ($\dot{\Omega}$) are given in

[1]Note that when the term 'frequency' is used a positive value is mentioned. In the real system and the simulation model this corresponds with a negative rotation direction!

equations (4.3) and (4.4):

$$\Omega(t) = \frac{H}{\Delta t}(t - t_0) - \frac{H}{2\pi}\sin\left(\frac{2\pi}{\Delta t}(t - t_0)\right) + \Omega(0), \tag{4.3}$$

$$\dot{\Omega}(t) = \frac{H}{\Delta t} - \frac{H}{\Delta t}\cos\left(\frac{2\pi}{\Delta t}(t - t_0)\right), \tag{4.4}$$

where:

H	'height' of the inclined sine function in Hz,
t_0	starting time of the inclined sine function in seconds,
Δt	duration of the inclined sine function ($t_{end} - t_{start}$) in seconds, and
$\Omega(0)$	angular velocity at $t = t(0)$ in Hz.

4.2 Estimate of the Friction Coefficient

To investigate the responses of the ABU system to an angular velocity setpoint, experiments have been carried out to determine some frequency dependent trend in the responses, resulting from the varying size of the equilibrium set as a function of the angular velocity. For frequencies between 10 and 28 Hz (in steps of 2 Hz), an angular velocity setpoint was applied in the steering program. This was repeated 10 times for each angular velocity. The results of one of these measurements can be seen in figure 4.1. An important observation is that the balls seem to settle (lie still) at an instant

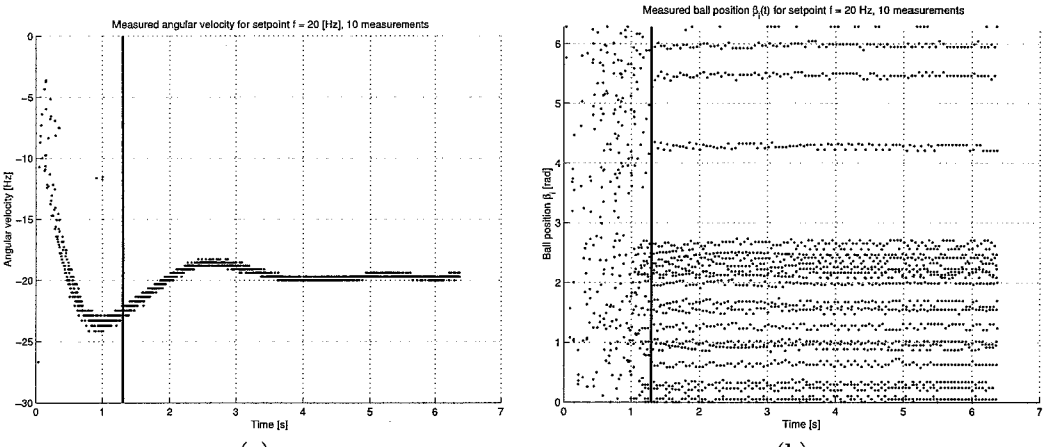

(a) (b)

Figure 4.1: Results for angular velocity setpoint of 20 Hz (10 measurements). Angular velocity is shown in (a), ball positions in (b). The settling time is approximately 1.3 seconds.

in time, immediately after the maximum rotational frequency overshoot (compare figure 4.1(a) and figure 4.1(b)). Unfortunately, however, no frequency dependent trend is discovered, as all target velocities yield similar results. This mean that with this motor control, it is not sensible to use a startup-profile built from setpoints.

After having implemented the simulation models, discussed in section 3.3.3, simulations have been performed using the *total ABU-model* to examine whether the simulation model can qualitatively capture the behaviour shown in figure 4.1. Simulations performed with a friction coefficient $\mu = 2.75 \cdot 10^{-3}$ (as given in section 3.1.4) show poor resemblance with the measured responses. Assuming that the influence of model errors or unmodeled dynamics is *not* the main cause for this discrepancy, it is likely that this is caused by a non-matching friction coefficient. To investigate this, simulations are carried out for various friction parameters: $\mu \in [2.75 \cdot 10^{-3}, 2.75 \cdot 10^{-2}]$. Figure 4.2 shows the simulation results for a setpoint of 20 Hz and friction coefficients of $\mu = 2.75 \cdot 10^{-3}$ and

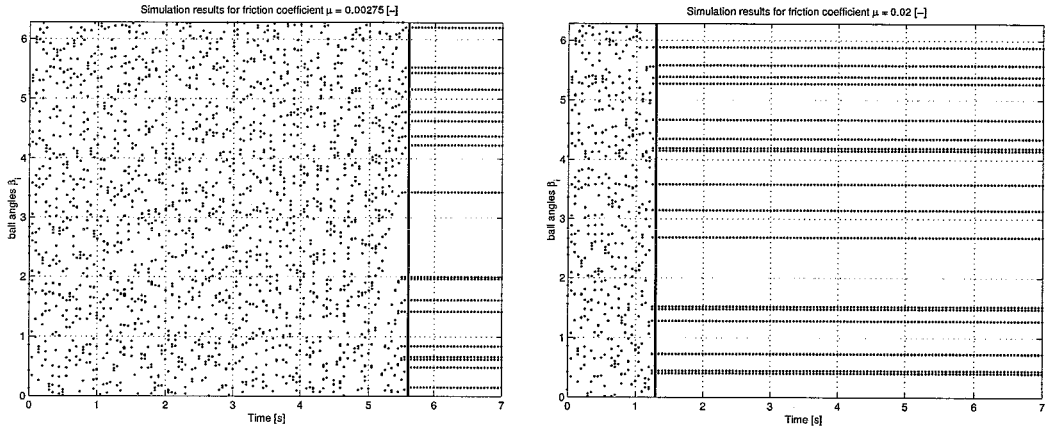

(a) (b)

Figure 4.2: Simulation results with angular velocity setpoint 20 Hz (9 simulations). Friction coefficient $\mu = 2.75 \cdot 10^{-3}$ (a) and $\mu = 0.02$ (b).

$\mu = 0.02$, respectively. It can be seen that there is quite a good matching of the settling times for the higher value of μ (figure 4.2(b)). For the other experiments, similar matching of the responses is observed by increasing the friction coefficient. For target velocities where the overshoot of the angular velocity crosses the natural frequency of the system ($f_n = 28.9$ Hz), also a settling in two steps is observed, both in experiments and simulations, for $\mu = 0.02$. This is caused by the phase difference on which the working principle of the ABU is based (see section 1.1). Therefore, from now on the following value for the friction coefficient is assumed:

$$\mu = 0.02 \text{ [-]}.$$

The value of μ obtained in this way is considered to be an educated guess for the friction coefficient. More meaningful simulations can now be performed to investigate the dynamic behaviour of the system. A recent study has shown that the friction coefficient is even larger (see [Suy03]).

4.3 Design of the First Part of the Startup-Profile

As already mentioned at the beginning of chapter 4, the startup-profile will roughly consist of two parts. The first part aims at obtaining reproducible ball positions and will be discussed next. The second part, an increase of the angular velocity to 100 Hz, will be discussed in section 4.4.

4.3.1 Obtaining Reproducible Ball Positions in One Step

Calculation of the equilibrium sets for various angular velocities for the newly obtained value of μ (= 0.02) shows that only very close to the systems natural frequency (28.94 Hz) these sets do *not* completely cover the β_1-β_2-plane. Close to the natural frequency of the system, there is namely a lot of vibrational energy in the system. With help of the simulation model, it is examined for which frequencies the set does not fill the entire β_1-β_2-plane. This takes place for frequencies $28.20 \leq f \leq 29.74$ Hz. In fact, this is the reason for the startup-profile to consist roughly of *two* parts. Namely, the first part will have its end frequency in this region. However, for the natural frequency of the system, the equilibrium set still is quite large, which can be seen in figure 4.3. The contour-lines in this figure indicate the vibrational amplitude $\sqrt{x^2 + y^2}$. In the equilibrium set also the two equilibrium *points* are located, namely $[\beta_1, \beta_2] = [4.0134, 2.2698]$ or vice versa. These points are the stable equilibrium points of the system without friction. They correspond with the darkest spots in figure 4.3.

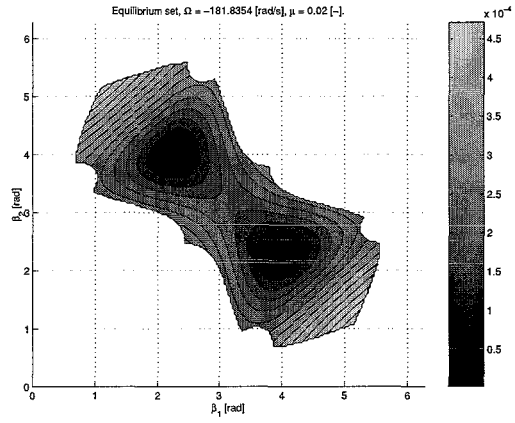

Figure 4.3: Equilibrium set at the natural frequency of the system ($f = 28.94$ Hz).

Moreover, simulations have been performed to investigate the influence of the parameters of the inclined sine function, namely duration and end-frequency. These simulations use 100 random initial conditions in the β_1-β_2-space and use inclined sine functions of various durations Δt (see equations (4.3) and (4.4)). It is observed that the influence on the equilibrium positions is most beneficial for a target frequency of $f = 29.5$ Hz. This is judged by calculating the residual imbalance, as defined in equation (4.2), averaged over all simulations. This measure appears to be smallest for the frequency mentioned. For this frequency, the influence of the inclined sine function is more thoroughly investigated. This is done by examining the influence of the duration Δt on the resulting equilibrium positions and settling times of the balls. (The settling time is defined as the time instant at which *both* balls lie still.)

For this purpose, 10 series of 1024 simulations have been carried out (initial conditions randomly chosen in a 32×32 grid in the $\beta_1(0)$-$\beta_2(0)$-space), in which the duration of the inclined sine function is varied between $\Delta t = 1$ and 10 seconds. In order to compare these series, the same 1024 initial conditions are used in each series. The results of one simulation series can be seen in figure 4.4.

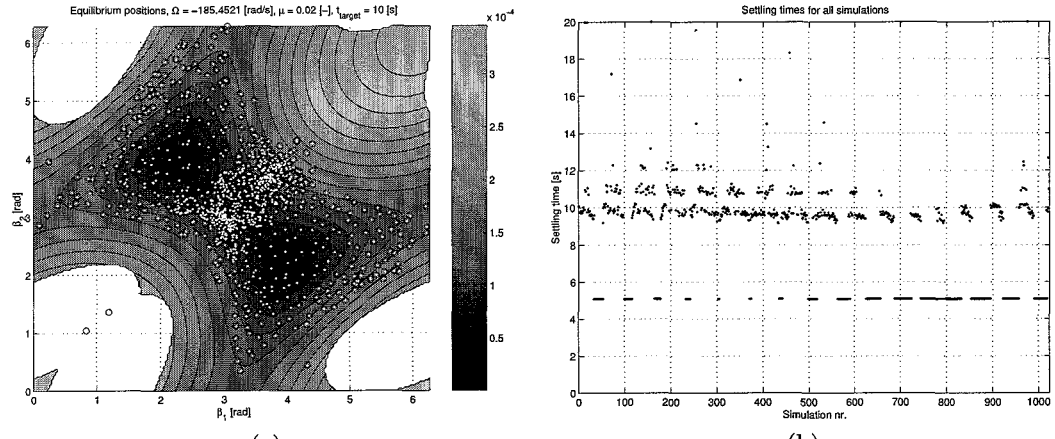

(a) (b)

Figure 4.4: Simulation results for inclined sine function to 29.5 Hz in $\Delta t = 10$ s. Equilibrium positions (a) and settling times (b) (Note: two simulations ended *outside* the equilibrium set, caused by (transient) limit cycle behaviour, as the limit cycle contains parts where β_i = constant).

The equilibrium positions β_i show clearly that some regions in the β_1-β_2-space are more crowded than others. Furthermore, it is observed that the settling times vary significantly. Roughly 40% of the simulations settles at about 5 seconds, whereas another 40% settles at the end time of the startup profile (10 seconds). In the rest of the simulations the settling times become even higher. Some simulations have transient behaviour of very long duration, possibly due to limit cycle behaviour. One logically would ask oneself *which* end positions β_i correspond with *which* settling times. The following general observation can be made: for all simulations carried out (Δt in the range of 1 to 10 seconds) the initial conditions $\beta_i(0)$ have great influence on the equilibrium positions. Results for $\Delta t = 10$ s can be seen in figure 4.5.

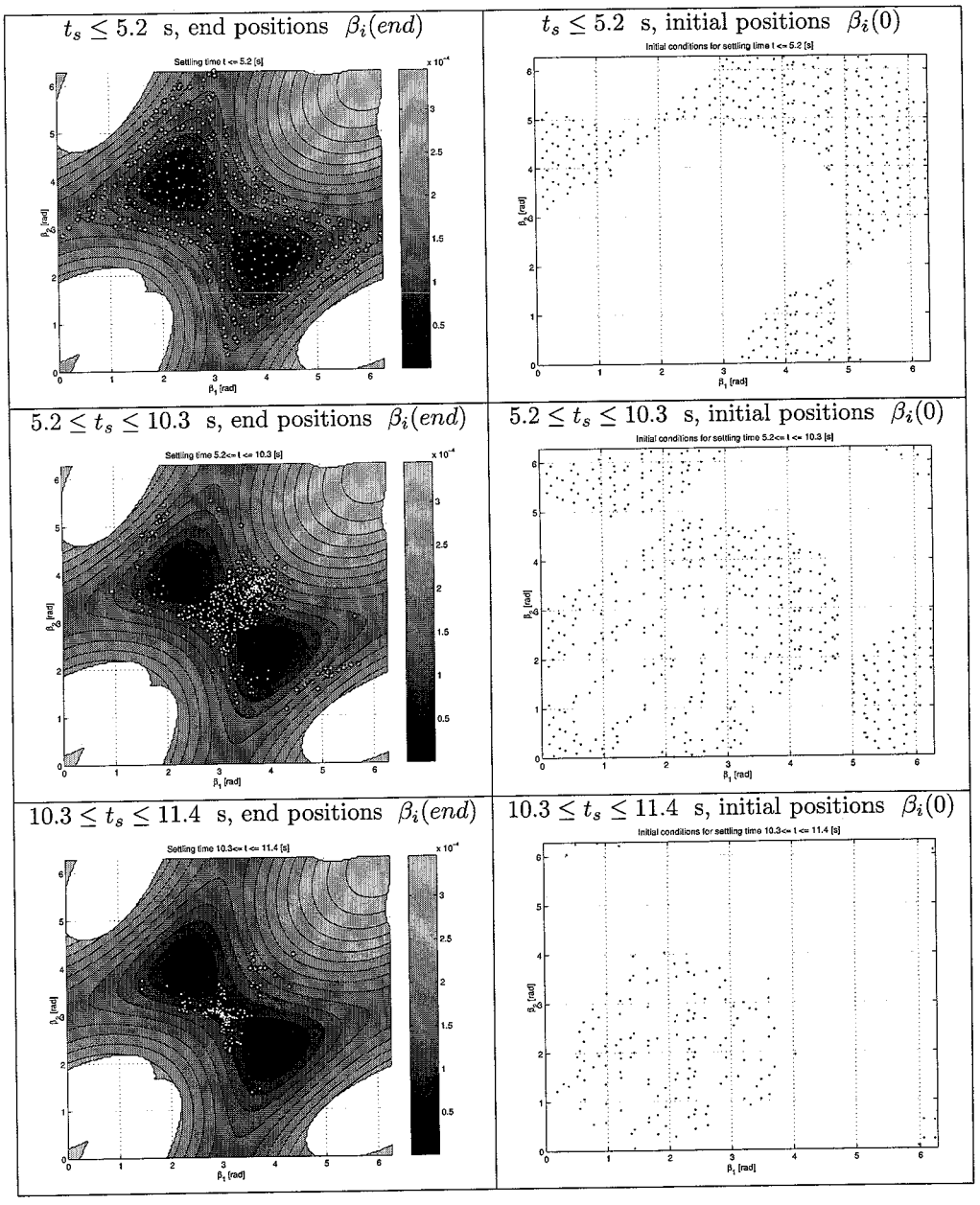

Figure 4.5: Dependency on initial conditions for $\Delta t = 10$ s.

Taking a closer look at the settling times, several observations can be made: the simulations in which there is a small settling time ($t_s \leq 5.2$ s) result in a sort of 'random' end positions in a *part* of the final equilibrium space. Note, however, that when the balls settle the startup-profile is *not* finished yet, but only half way. At this time instant the angular velocity of the profile is about 15 Hz. Furthermore, the balls in the simulations with a settling time slightly larger than the profile end-time ($t_s \approx 10$ s) obtain quite a reproducible position. Also the next settling time belongs to reproducible positions. Somehow, it may be possible to make advantage of this 'sorting' property of the system.

Another observation shows up when the initial conditions belonging to the corresponding settling times are plotted (the second column in figure 4.5). The system shows dependency on the initial conditions $\beta_i(0)$, namely the settling times for two initial conditions close to each other, can vary significantly. Moreover, the position of the initial condition regions varies with the inclined sine duration Δt. It is known from the simulations that *all* balls lie still at 5.2 s. Therefore, a possible explanation for the initial condition dependency is the following: all balls settling the first time (at $t = 5.2$ s) in regions outside the region bounded by the equilibrium points depicted in the top-left picture of figure 4.5, start rolling again. This phenomenon is possibly due to the phase difference on which the working principle of the ABU is based.

Furthermore, it is observed that the balls rarely settle at the ideal balancing position, meaning that there is little driving force towards these points. This implies that these equilibrium points are not as attracting as desired (at least for this profile).

The results of the simulations performed are given in table 4.1, where $\frac{1}{n}\sum I_r$ denotes the *mean* residual imbalance, $\%LC$ denotes the percentage limit cycles, and $\%MI$ the percentage simulations resulting in more imbalance than without balls (defined by $I_r \geq I$) (see equation (4.1) and (4.2) for explanation). Note: the balls are *defined* to be in a limit cycle if at the simulation end time (twice the profile end time) no equilibrium is found. This does *not* imply that the balls are actually in a limit cycle, but it is more or less an upper bound for the transient behaviour of the first part of the profile.

Table 4.1: Simulation results for the one-step profile to 29.5 Hz (the large maximum residual at $\Delta t = 10$ s results from the two end positions outside the equilibrium set (see figure 4.4(a))).

Δt [s]	$\frac{1}{n}\sum I_r$ 10^{-7} [kg m]	I_r max. 10^{-7} [kg m]	$\%LC$	$\%MI$
1	11.54	44.65	0	15.43
2	11.41	33.47	0	15.43
3	10.05	30.89	0.49	11.04
4	10.00	28.52	1.37	9.18
5	9.76	28.28	0.49	8.69
6	9.57	27.99	0.49	7.23
7	9.67	27.35	1.07	6.35
8	9.76	27.64	2.05	5.76
9	9.49	26.86	1.07	5.27
10	9.37	39.67	1.46	5.47

The following observations can be made from table 4.1. The general trend is that a longer profile duration results in less mean imbalance *and* a smaller percentage of simulations with more imbalance than the system without balls. Therefore, it appears to be beneficial to use a startup-profile with long time duration Δt. Moreover, as can be seen in figure 4.5, simulations in which the balls start rolling again ($t_s \geq 5.2$ s) result in more reproducible end positions than the ones in which the balls lie still from this time instant (see figure 4.5).

From these two observations it is concluded that a slow transition through the natural frequency of the ABU system ($f_n = 28.9$ Hz) has a beneficial influence on the equilibrium position of the

balls, as both the equilibrium set is smallest for this frequency and there is more vibrational energy in the system, driving the balls to 'better' positions (compare the bottom two pictures in the left column of figure 4.5 with the top one). Therefore, the first part of the profile is split up in two steps, which will be discussed in the next paragraph.

4.3.2 Obtaining Reproducible Ball Positions in Two Steps

As mentioned in the previous section, the first part of the startup-profile is split up in two steps. The first step consists of a fast increase in angular velocity to a frequency below the natural frequency, as this step is not considered to be the crucial step in the profile. The second step (slowly) increases the angular velocity to 29.5 Hz. Care must be taken however that such a slow transition through the natural frequency could potentially harm the system as large vibrations are induced in this way.

To investigate the response of the system to this two-step profile, simulations are carried out using a profile which consists of two inclined sine functions to a frequency below (f_1) and a frequency above (f_2) the eigenfrequency. After some initial simulations the first frequency is chosen $f_1 = 25$ Hz and the second frequency remains unchanged with respect to section 4.3.1: $f_2 = 29.5$ Hz. The first step duration is set to $\Delta t = 1$ s, which implies that *all* balls are still rolling at the end time of the first step. The second step time duration is varied between 2 and 10 seconds. Results (1024 simulations for each Δt_2) are depicted in figure 4.6.

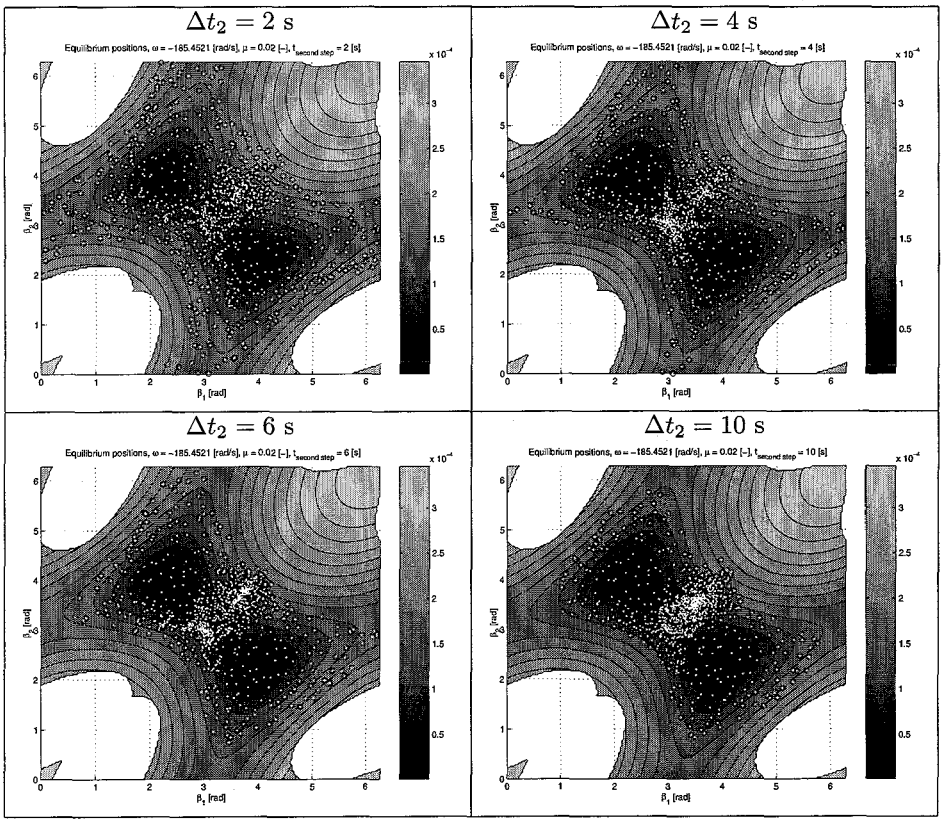

Figure 4.6: Results for the two-step startup-profile with $\Delta t_1 = 1$ s and Δt_2 variable.

To simplify the interpretation the results are also given in table 4.2. From these results, it is observed that a larger second step time has positive influence on the ball positions and $\%MI$, as was also the case in section 4.3.1. An increasing Δt_2 namely results in a smaller mean residual

Table 4.2: Simulation results for the two-step profile to 29.5 Hz. $f_1 = 25$ Hz, $\Delta t_1 = 1$ s, $f_2 = 29.5$ Hz and $\Delta t_2 =$ variable.

Δt_2 [s]	$\frac{1}{n}\sum I_r$ 10^{-7} [kg m]	I_r max. 10^{-7} [kg m]	$\%LC$	$\%MI$
2	9.87	28.43	6.05	8.79
4	9.33	28.07	3.03	4.79
6	8.67	25.71	2.54	3.32
8	8.75	25.71	1.17	2.25
10	8.85	24.67	0.49	1.56

imbalance. For $\Delta t_2 \geq 4$ s, the mean residual imbalance and $\%MI$ is better than the one-step startup-profile from the previous section (see table 4.1). This justifies the splitting up of the first part of the profile.

Considering these results, it can be stated that a suitable first part of the profile is designed. Reproducible positions of the balls are obtained by using $f_1 = 25$ Hz, $\Delta t_1 = 1$ s, $f_2 = 29.5$ Hz and $\Delta t_2 = 10$ s. Note that $\%MI$ is considered to be more important[2] here than $\frac{1}{n}\sum I_r$. In the second part of the startup-profile, these equilibrium positions are to be kept unchanged as much as possible. This will be discussed next.

4.4 Increasing the Angular Velocity to the Target Frequency

As mentioned in section 4.1.1, the target frequency of the startup-profile is 100 Hz. With the first part of the profile designed, some kind of speeding up has to take place such that the balls approximately remain at their position. This implies that it is assumed that the results with the profile up till now are considered to be the best results attainable with the inclined sine function. This is a major assumption, but from the results so far, it is clear that the ideal balancing position will not be attained using this profile. This more or less justifies the assumption and, more important, an improvement with respect to no balancing has actually occurred.

In order to investigate the speeding up to the target frequency, the profile is extended to a three-step profile with inclined sine functions from 29.5 to 100 Hz of varying duration. Eight series of 256 simulations are performed for durations between 1 and 20 s. The results of this analysis can be seen in table 4.3. Note that at a frequency of 100 Hz no limit cycles occur (all simulations end in equilibrium), thus the column $\%LC$ is omitted.

Table 4.3: Simulation results for the three-step profile to 100 Hz.

Δt_3 [s]	$\frac{1}{n}\sum I_r$ 10^{-7} [kg m]	I_r max. 10^{-7} [kg m]	$\%MI$
1	9.37	47.41	3.13
2	9.35	37.22	3.52
3	9.22	43.93	2.73
4	8.74	27.37	3.13
8	8.53	25.56	2.34
12	8.61	25.56	2.73
16	8.64	25.56	3.13
20	8.55	25.56	2.34

[2] An ABU manufacturer would want to guarantee a certain reliability percentage for the startup-profile. $\%MI$ gives an indication for the failure percentage.

Carefully looking at table 4.3, yields the conclusion that the results are quite reproducible for $\Delta t_3 \geq 4$ s. For these time durations the results do not vary a lot. Below 4 seconds however, there is a substantial increase of the mean residual imbalance and the maximum residual imbalance. From these results, the duration of $\Delta t_3 = 8$ yields the smallest mean residual imbalance and the smallest $\%MI$. Therefore, this duration is proposed to complete the startup-profile.

Before the final choice of the startup-profile is made, however, a comparison has to take place between the three-step startup-profile and a one-step profile (of varying duration) to the target frequency. This comparison is given in table 4.4, where for the one-step profile also series of 256 simulations were performed. For a fair comparison also a one-step startup-profile is applied which has the same duration as the three-step profile, namely 19 seconds.

Table 4.4: Comparison between the three-step startup-profile and a one-step profile to a target frequency of 100 Hz.

Profile	Δt_{total} [s]	$\frac{1}{n}\sum I_r$ 10^{-7} [kg m]	I_r max. 10^{-7} [kg m]	$\%MI$
three-step	19	8.53	25.56	2.34
one-step	2	25.11	52.34	61.33
	4	20.73	52.60	41.02
	6	12.78	51.95	19.14
	8	21.49	52.56	45.70
	10	20.20	49.48	47.66
	19	17.13	50.25	37.11

The comparison of the three-step and one-step profile of equal lengths is also depicted in figure 4.7. Note that no equilibrium set is plotted, as the equilibrium set at 100 Hz covers the β_1-β_2-plane completely.

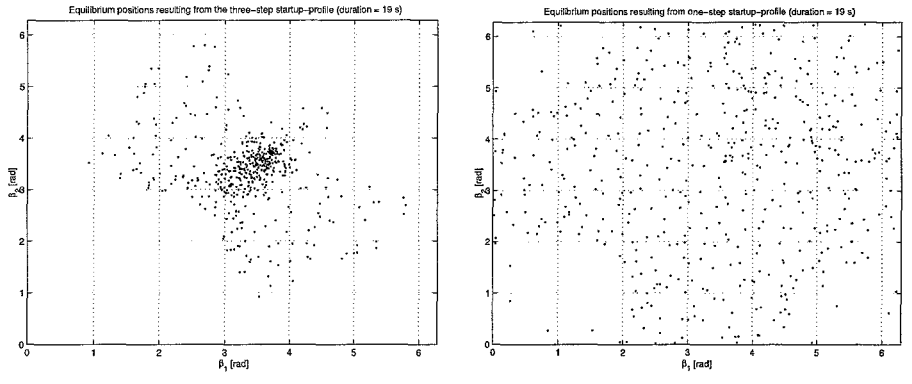

Figure 4.7: Comparison between equilibrium positions of the three-step profile (a) and the one-step profile (b). Both profiles have equal time durations, namely 19 seconds.

From table 4.4, it follows that the three-step startup-profile gives much better results than the one step profile, which justifies the design approach followed. Namely, only close to the natural frequency of the system one can have influence on the ball positions. Therefore, the proposed third step duration is accepted and the final startup-profile is the following:

From	$f = 0$ to $f = 25$ Hz	in $\Delta t_1 = 1$ s,
from	$f = 25$ to $f = 29.5$ Hz	in $\Delta t_2 = 10$ s, and
from	$f = 29.5$ to $f = 100$ Hz	in $\Delta t_3 = 8$ s.

Furthermore, a large number of simulations (1024 initial conditions) have been performed to obtain more accurate values for the quantities given in table 4.4. This yields:

Mean residual imbalance	$\frac{1}{n}\sum I_r$	=	$8.96 \cdot 10^{-7}$ kg m,
Maximum residual imbalance	I_r max.	=	$24.45 \cdot 10^{-6}$ kg m,
Percentage with more imbalance than I	$\%MI$	=	1.56%.

4.5 Sensitivity of the Startup-Profile

From robustness considerations, it is desired to investigate the sensitivity of the startup-profile to a great diversity of parameters/influences. Due to the fact that the optimization tool from the ADOPT project is not ready yet, only the sensitivity of the startup-profile to the friction coefficient μ is investigated, because an educated guess for its value was proposed in section 4.2. From a recent study to determine the friction coefficient (see [Suy03]), it is known that the friction coefficient has approximately a value of $\mu = 0.03$. This value has only recently been determined. Therefore, this value was not used during the design process of the startup-profile. Here, it is decided to vary the friction coefficient in the range $\mu \in [0.02, 0.04]$ and examine its influence on the equilibrium positions of the balls. This is also useful as a friction coefficient is not a fixed value, but changes under various influences. Ageing of the ABU-system could cause, for instance, an increase of μ due to deterioration of the surface quality of the balls and wear of the rim of the ABU. The results are presented in figure 4.8, for two values of μ.

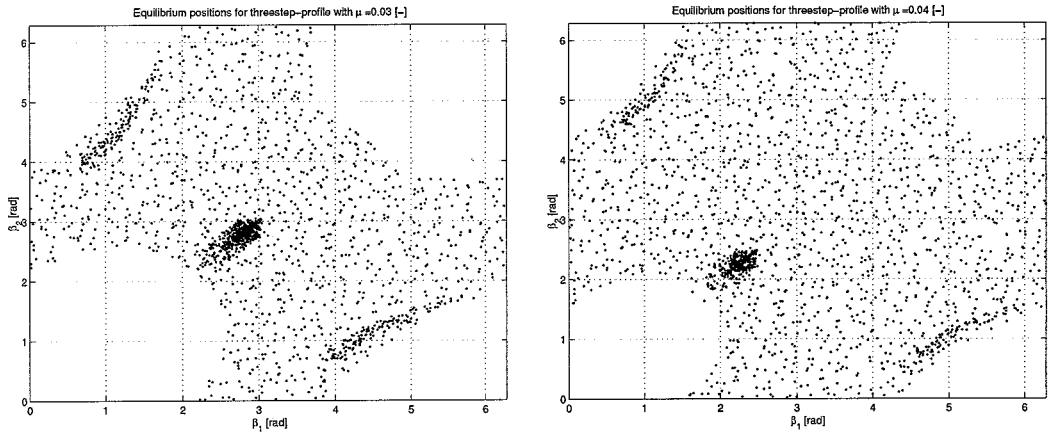

(a) (b)

Figure 4.8: Sensitivity of the equilibrium positions for the friction coefficient. $\mu = 0.03$ [-] (a) and $\mu = 0.04$ [-] (b).

The dependency on the friction coefficient of the mean residual imbalance and the percentage simulations with more imbalance than without balls, is also investigated and depicted in figure 4.9.

From figures 4.8 and 4.9, it follows that a higher value of the friction coefficient has a negative effect on the resulting equilibrium positions. In optimization procedures that will be carried out in the future (ADOPT) this could possibly also be taken into account. For this study, it is merely mentioned that the dependency exists.

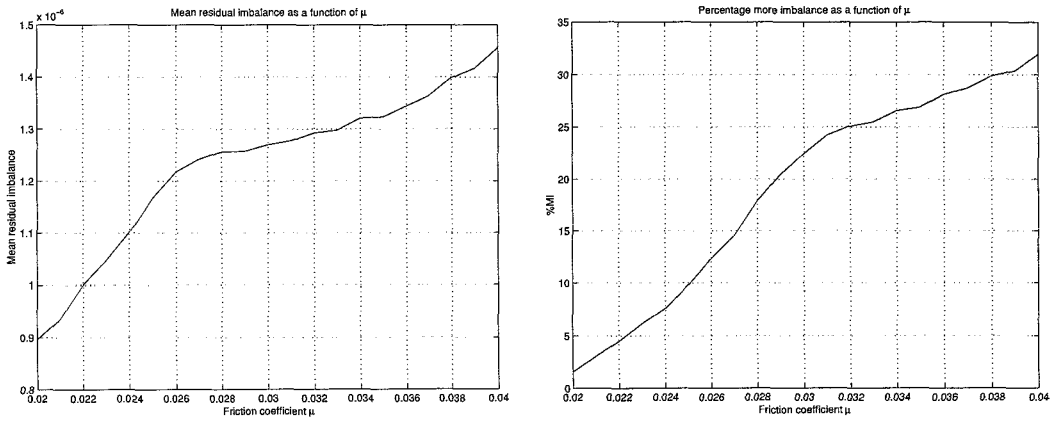

(a) (b)

Figure 4.9: Dependency on the friction coefficient. Mean residual imbalance (a), $\%MI$ (b).

4.6 Optimization Problem Layout

The method, with which the startup-profile is designed in this chapter, is in fact a manual optimization in which several choices and assumptions were made, based on educated guesses. With the optimization tool that is currently being developed in the ADOPT project, a more thorough optimization could be performed, taking into account as much parameters as one would like (within computation time restrictions).

In an optimization problem, an objective function should be minimized or maximized (dependent on the kind of problem). In this chapter, two kinds of functions were used, which were somehow minimized (by hand), namely the mean residual imbalance and the percentage of the simulations resulting in an increase in imbalance. For a real optimization, possibly a combination of these quantities could be used as an objective function.

Furthermore, an optimization problem in general will be subject to constraints (this is certainly the case for optimization of mechanical products or systems). A maximum allowable startup time could serve as a possible constraint, or, for instance, a maximum vibrational amplitude at the transition through the natural frequency of the system could be formulated. It could also be demanded, that in at least a certain percentage of the application of the startup-profile, say 95%, the imbalance of the system is reduced, thus formulating an upper bound on $\%MI$.

Moreover, simulations with the *ABU-model* require a large computational effort. The computation time could greatly be reduced by designing Response Surface Models (RSM) to approximate the behaviour of the system (see for example [RE02]). This is however only possible if the responses of the system are not discontinuous, but smooth. Figure 4.9 shows that there is indeed such dependency on for example the friction coefficient. A possible difficulty that could arise here is that there is an initial condition dependency of the equilibrium positions (see section 4.3.1). Otherwise, even another strategy could be used, namely sequential approximate design optimization (see also [RE02]), which consists of an iterative refinement and design of RSM models.

Chapter 5

Conclusions and Recommendations

In order to design a 'smart' startup-profile for the ABU, first of all two models for the ABU system have been constructed, one including the motor behaviour (*total ABU-model*) and one without the motor behaviour (*ABU-model*). These models have been numerically implemented in the programming package MATLAB. By means of matching of the settling times (durations in which both balls attain their equilibrium position) between the experiments and the *total ABU-model* during a setpoint profile, an estimate of the friction coefficient is made, which differs significantly from the one in [Heu02]. This value is used throughout the project; $\mu = 0.02$.

Furthermore, due to non-reproducibility of the responses of the motor system and due to the steering program, which is incapable of handling smooth functions, the motor dynamics are considered to be less important in the design process of the startup-profile. Therefore, an ideal motor control is assumed, justifying the use of the *ABU-model.* However, this means that the startup-profile cannot be tested on the experimental setup.

Using the friction coefficient estimate, it is investigated how the size of the equilibrium set varies for frequencies around the natural frequency of the system (28.9 Hz). This set does not cover the complete β_1-β_2-plane for frequencies $f \in [28.20, 29.74]$ Hz. This implies that the startup-profile should make use of this frequency dependent size of the equilibrium set and, therefore, it consists of two parts. The first part will end at a frequency in this frequency region and aims at obtaining reproducible ball positions. The second part consists of an increase of the angular velocity to the target frequency ($f = 100$ Hz).

Several design criteria and assumptions for the startup-profile have been formulated, as the problem consists in fact of a manual optimization problem, in which a lot of choices have to be made. First, the mean residual imbalance should be as small as possible. Secondly, the startup-profile should yield reproducible results. A measure for this is defined as a small percentage of simulations resulting in more imbalance than the system without balls. Furthermore, a general choice for the form of the startup-profile is made, namely an inclined sine function. Next, it is investigated for which angular velocity, in the frequency region of interest, there is large influence on the resulting ball positions using the inclined sine function. The results shows that there is large influence at an angular velocity of 29.5 Hz.

Numerous time simulations have been performed with inclined sine functions of various durations to this angular velocity. From these simulations it appears that a slow transition through the natural frequency ($f = 28.9$ Hz) of the system is beneficial. Due to a small equilibrium set around this frequency and more vibrational energy in the system, the balls are driven to 'better' positions. Moreover, an initial condition dependency is observed, for which no satisfactory explanation has been found.

Next, the part of the startup-profile that ends at a rotational velocity of 29.5 Hz (the first part) is split into two parts. An inclined sine function to increase the angular velocity to 25 Hz with a

duration of 1 s, followed by an increase to 29.5 Hz in 10 s, is shown to be more effective compared to one inclined sine function to this frequency. Namely, a small mean residual imbalance is obtained, as well as a small percentage of simulations resulting in more imbalance than the system without balls.

Next, the second part of the startup-profile is designed. An inclined sine function with a duration of 8 s gives satisfactory results. After comparison with a one-step startup-profile to 100 Hz the final choice for the startup-profile is made: the two part-startup profile, consisting of three inclined sine functions. Moreover, the sensitivity of the startup-profile to the friction coefficient has been investigated. This sensitivity is shown to be quite significant.

Finally, a general layout for an optimization problem on the ABU is formulated, which could be used with an optimization tool currently being developed in the ADOPT project.

To improve the insight in the dynamic behaviour of the ABU system, to check the validity of the model and to test the startup-profile, several recommendations can be made.

First, it was not possible to test the designed startup-profile on the experimental setup, due to difficulties with the motor control (non-reproducibility and discretization). An other steering program in combination with an other motor control could make this testing possible.

Furthermore, other choices than inclined sine functions could be made to design the startup-profile. In this project, this restriction was made to keep the number of variables in the profile within a reasonable bound.

Finally, it could be investigated whether the change of phase between the rotor and the imbalance is the cause for the initial condition dependency observed in the simulations using one inclined sine function to 29.5 Hz. A thorough understanding of the cause of this dependency could greatly help in the design process of the startup-profile as one could possible take this behaviour into account or compensate for it.

Bibliography

[Heu02] M.N. van den Heuvel, *Modeling and Analysis of an Automatic Balancing Unit with Dry Friction*, Master's thesis, Eindhoven: Eindhoven University of Techonology, Department of Mechanical Engineering, DC-Report No. 2002-67, 2002.

[Koe01] A.H. Koevoets, *Dynamics of an Automatic Dry Ball Balancer applied to a Disk System*, Master's thesis, Eindhoven: Eindhoven University of Techonology, Department of Mechanical Engineering, DC-Report No. 2001-28, 2001.

[Lei00] R.I. Leine, *Bifurcations in Discontinuous Mechanical Systems of Fillipov-Type*, Ph.D. thesis, Eindhoven: Eindhoven University of Techonology, Department of Mechanical Engineering, 2000.

[Phi02] Philips Optical Storage, *Documentation Motor Control:* `readme.txt`, 2002.

[RE02] J.J.M. Rijpkema and L.P.F. Etman, *Engineering optimization: Advanced topics*, Eindhoven: Eindhoven University of Techonology, Department of Mechanical Engineering, Lecture Notes, 2002.

[Suy03] H.M.R. Suy, *Measurement of the static friction coefficient in an automatic balancing unit with dry friction*, Eindhoven: Eindhoven University of Techonology, Department of Mechanical Engineering, DC-Report No. 2002-22, 2003.

[Wou02] N. van de Wouw, *Multibody dynamics*, Eindhoven: Eindhoven University of Techonology, Department of Mechanical Engineering, Lecture Notes, 2002.

Appendix A

Measurement Example

As an elucidation on the measurement method using the optical sensor, an example is provided next. For this purpose, an angular velocity setpoint is prescribed in the steering program. Using a SIGLAB measurement interface, the signal from the optical sensor is measured and sampled at 1280 Hz, which renders a total measurement time of approximately 6.4 s, due to memory capacity of the data acquisition interface. A part of the measured signal can be seen in figure A.1. In

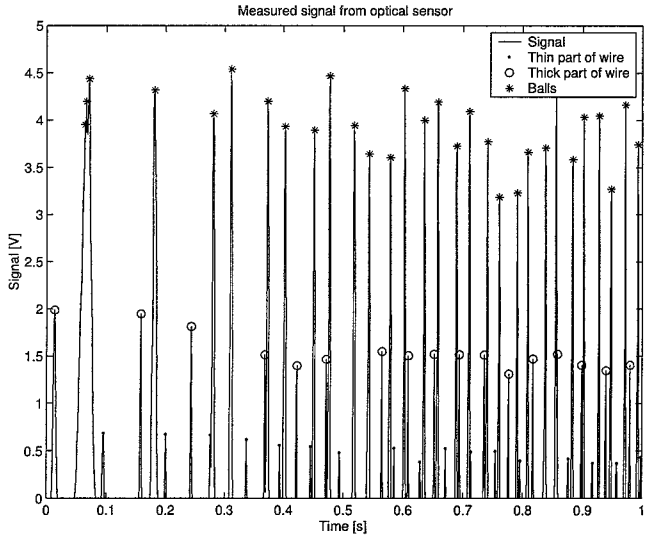

Figure A.1: Part of the measured signal from the optical sensor.

MATLAB a kind of interpolation algorithm is written that analyses the measurements and extracts the angular velocity and the ball angles β_i $(i = 1, 2)$ from this signal. The extracted rotational velocity and ball angles can be seen in figures A.2 and A.3.

Figure A.2 shows that the angular velocity can only be extracted at discrete instants in time. Moreover, in figure A.3 it can be seen that only after settling of the balls one can see which ball is which. During the first part (for $t \leq 1$ s), it is not clear which ball is which because of movement of the balls relative to the ABU. In the interpolation algorithm it is assumed that only relative movement with respect to the ABU in one direction takes place and that no collisions between the balls occur. Therefore, the interpolation algorithm is not ideal for extracting the transient behaviour of the balls, but another method was not found.

Finally, as mentioned in section 2.2, the accuracy with which the ball positions can be reconstructed depends on the rotational velocity and the sampling frequency of the optical sensor data. At a sample frequency of f_s Hz and a rotational frequency of f_{real} Hz, the resolution with which

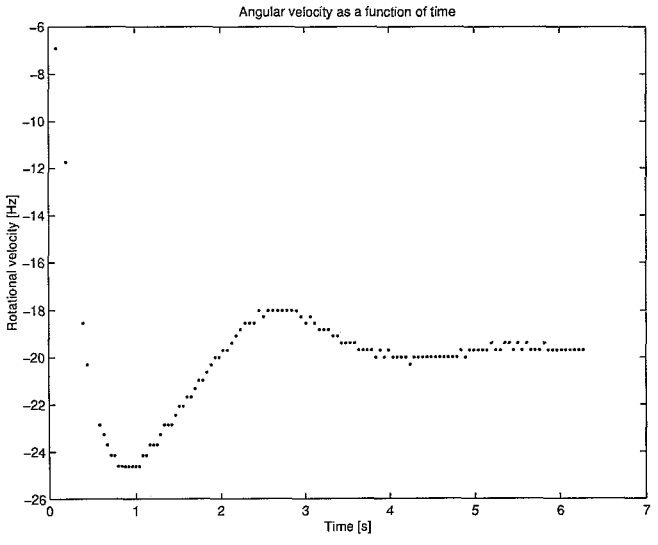

Figure A.2: Angular velocity, extracted from measurement.

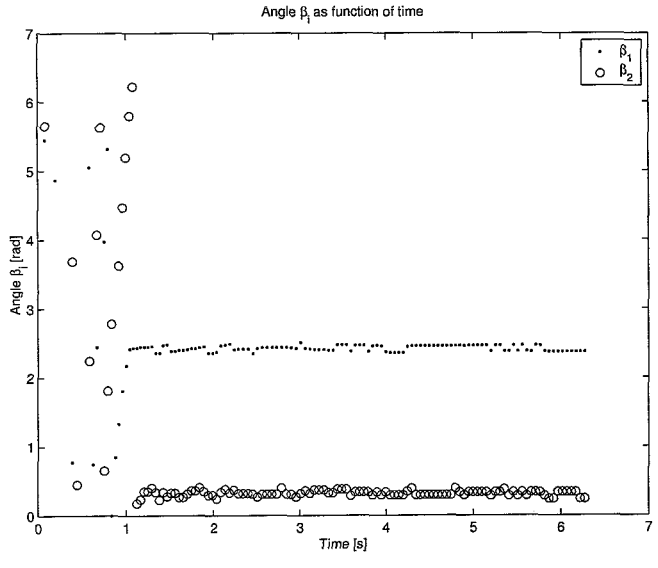

Figure A.3: Ball angles β_i $(i = 1, 2)$, extracted from measurement.

the angular position of the balls (in radians) is determined follows from:

$$\Delta\beta = 2\pi \frac{f_{real}}{f_s}. \tag{A.1}$$

For the stationary part of the measurement ($t \geq 5$ s) $f_{real} \simeq 20$ Hz and $f_s = 1280$ Hz, which yields an accuracy of $\Delta\beta = 0.196$ rad or 5.63°, which can also be seen in figure A.3.

In figure A.2, it can also be seen that the motor realizes the frequency setpoint with a large overshoot. In section 3.2.3 it will be shown that this is a very undesired motor (control) characteristic, evenmore so because this behaviour is non-reproducible.

Appendix B

Derivation of the Equations of Motion of the ABU

B.1 Kinematics of the Model

In order to derive the equations of motion, first the kinematics of the ABU-model have to be elaborated. This elaboration depends on the choice of generalized coordinates. As already mentioned in chapter 3 the (real) generalized coordinates are chosen as $\underline{q}_r = \begin{bmatrix} x & y & \beta_1 & \beta_2 & l_1 & l_2 \end{bmatrix}$ (see figure B.1).

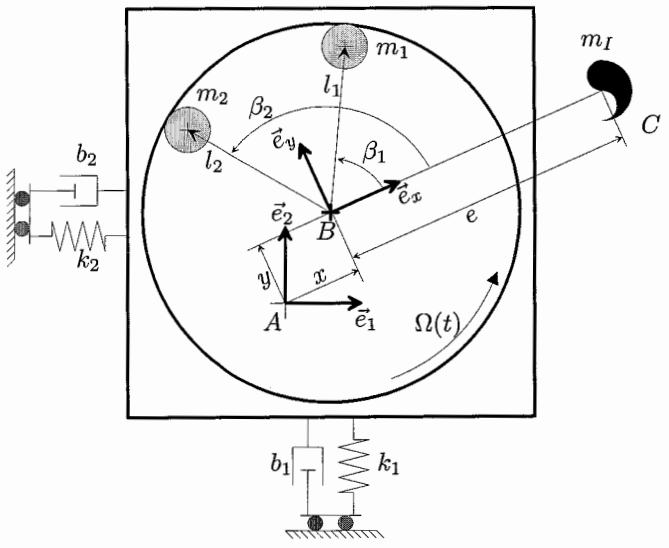

Figure B.1: Schematic model of the ABU.

Using figure B.1, this choice leads to the following expressions for describing the positions of the elements in the ABU:

$$\vec{r}_{AB} = \begin{bmatrix} x & y \end{bmatrix} \begin{bmatrix} \vec{e}_x \\ \vec{e}_y \end{bmatrix}, \tag{B.1}$$

$$\vec{r}_{AC} = \vec{r}_{AB} + e\ \vec{e}_x, \tag{B.2}$$

$$\vec{r}_{Am_i} = \vec{r}_{AB} + \begin{bmatrix} l_i \cos\beta_i & l_i \sin\beta_i \end{bmatrix} \begin{bmatrix} \vec{e}_x \\ \vec{e}_y \end{bmatrix},\ i = 1, 2. \tag{B.3}$$

Furthermore, the rotation from the inertial frame, $\underline{\vec{e}}^0 = \begin{bmatrix} \vec{e}_1 \\ \vec{e}_2 \end{bmatrix}$, to the body-fixed frame of the ABU, $\underline{\vec{e}}^1 = \begin{bmatrix} \vec{e}_x \\ \vec{e}_y \end{bmatrix}$, can be described using the direction cosine matrix $\underline{A}^{10}$:

$$\begin{bmatrix} \vec{e}_x \\ \vec{e}_y \end{bmatrix} = \underline{A}^{10} \begin{bmatrix} \vec{e}_1 \\ \vec{e}_2 \end{bmatrix} = \begin{bmatrix} \cos\theta(t) & \sin\theta(t) \\ -\sin\theta(t) & \cos\theta(t) \end{bmatrix} \begin{bmatrix} \vec{e}_1 \\ \vec{e}_2 \end{bmatrix}, \tag{B.4}$$

where

$$\theta(t) = \int_0^t \Omega(\tau)d\tau + \theta(0). \tag{B.5}$$

For the rest of the derivation $\theta(0)$ is assumed to be zero.

Differentiating these position vectors with respect to time yields the velocity vectors. To compute the derivative of the body fixed frame of the ABU with respect to time, equation (B.6) is used:

$$\dot{\underline{\vec{e}}}^1 = -{}^{10}\underline{\tilde{\omega}}^1 \underline{\vec{e}}^1 = {}^{10}\vec{\omega} \times \underline{\vec{e}}^1, \tag{B.6}$$

where the angular velocity vector ${}^{10}\vec{\omega}$ is given by:

$${}^{10}\vec{\omega} = \frac{d}{dt}\left(\theta(t)\right)\vec{e}_3^0 = \frac{d}{dt}\left(\theta(t)\right)\vec{e}_z^1 = \frac{d}{dt}\left(\int_0^t \Omega(\tau)d\tau\right)\vec{e}_3^0 = \Omega(t)\vec{e}_z^1, \tag{B.7}$$

with $\vec{e}_3^0 = \vec{e}_1^0 \times \vec{e}_2^0$ and $\vec{e}_z^1 = \vec{e}_x^1 \times \vec{e}_y^1$ the third components of orthonormal right-handed bases $\underline{\vec{e}}^0$ and $\underline{\vec{e}}^1$, respectively. From (B.7) it follows that ${}^{10}\vec{\omega} = \begin{bmatrix} 0 & 0 & \Omega(t) \end{bmatrix} \underline{\vec{e}}^1$ and, therefore,

$$\dot{\underline{\vec{e}}}^1 = \begin{bmatrix} \dot{\vec{e}}_x \\ \dot{\vec{e}}_y \end{bmatrix} = \begin{bmatrix} \Omega(t)\vec{e}_y \\ -\Omega(t)\vec{e}_x \end{bmatrix}. \tag{B.8}$$

For simplicity, $\Omega(t)$ from now on will be written as Ω, with the explicit time-dependency kept in mind. The velocity vectors then become:

$$\dot{\vec{r}}_{AB} = \begin{bmatrix} \dot{x} - y\Omega & \dot{y} + x\Omega \end{bmatrix} \begin{bmatrix} \vec{e}_x \\ \vec{e}_y \end{bmatrix}, \tag{B.9}$$

$$\dot{\vec{r}}_{AC} = \begin{bmatrix} \dot{x} - y\Omega & \dot{y} + x\Omega + e\Omega \end{bmatrix} \begin{bmatrix} \vec{e}_x \\ \vec{e}_y \end{bmatrix}, \tag{B.10}$$

$$\dot{\vec{r}}_{Am_i} = \begin{bmatrix} \dot{x} - y\Omega - \dot{\beta}_i l_i \sin\beta_i - \Omega l_i \sin\beta_i + \dot{l}_i \cos\beta_i \\ \dot{y} + x\Omega + \dot{\beta}_i l_i \cos\beta_i + \Omega l_i \cos\beta_i + \dot{l}_i \sin\beta_i \end{bmatrix}^T \begin{bmatrix} \vec{e}_x \\ \vec{e}_y \end{bmatrix}, \; i = 1, 2. \tag{B.11}$$

Moreover, for the kinetic energy of the balls, which is to be derived in section B.2, the rotational velocity of the balls is needed. First, the rotation angle of the ball has to be derived. This angle follows from a no-slip condition between the ball and the rim of the ABU, which means that the relative velocities between the *contacting* surfaces are zero. From figure B.2 the following relation for the rotation angle of the ball is derived:

$$\alpha_i = -\beta_i \left(\frac{2l_i}{d_i} + 1\right), \; i = 1, 2. \tag{B.12}$$

Furthermore, the ball *rolls* in the ABU, which has a circular shape and a prescribed rotation $\Omega(t)$. Therefore the ball has an additional rotation of $\left(\beta_i + \int_0^t \Omega(\tau)d\tau\right)$. The total rotation then becomes:

$$\alpha_i = -\beta_i \left(\frac{2l_i}{d_i} + 1\right) + \beta_i + \int_0^t \Omega(\tau)d\tau = -\beta_i \frac{2l_i}{d_i} + \int_0^t \Omega(\tau)d\tau, \; i = 1, 2. \tag{B.13}$$

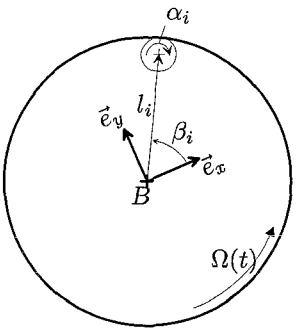

Figure B.2: Rotation angle of ball i.

Calculating the derivative of the ball angle (B.13) with respect to time, yields the angular velocity vector $\vec{\omega}_i$. Use is made of the time-derivative of (B.5) as elaborated in (B.7):

$$\vec{\omega}_i = \left(\Omega - \frac{2l_i}{d_i}\dot{\beta}_i\right)\vec{e}_z, \; i = 1, 2. \tag{B.14}$$

B.2 Kinetic and Potential Energy

After elaborating the kinematics, the kinetic and potential energy of the system can be calculated. The kinetic energy of the total system is given by:

$$T = \frac{1}{2}M_T\dot{\vec{r}}_{AB}\cdot\dot{\vec{r}}_{AB} + \frac{1}{2}m_I\dot{\vec{r}}_{AC}\cdot\dot{\vec{r}}_{AC} + \sum_{i=1}^{2}\left(\frac{1}{2}m_i\dot{\vec{r}}_{Am_i}\cdot\dot{\vec{r}}_{Am_i} + \frac{1}{2}J_i\vec{\omega}_i\cdot\vec{\omega}_i\right), \tag{B.15}$$

with M_T total mass of the system without imbalance and balls [kg],
m_I mass of the imbalance [kg],
m_i mass of ball i [kg],
J_i moment of inertia of ball i around its center of mass, given by $J_i = \frac{1}{10}m_i d_i^2$ [kg m^2].

Furthermore, a term containing the kinetic energy due to rotation of the CD-ROM disc should be noted in equation (B.15). As this term ($\frac{1}{2}J_{disc}\Omega^2$) contains no generalized coordinates it will not show up in the final equations of motion. Moreover, the assumption is made that rotation of total system around the $\vec{e}_z$-direction does *not* take place. This means that the generalized coordinates x and y suffice to describe the position of point B in figure B.1.

The potential energy of the system is only composed of energy stored in the springs k_1 and k_2, as gravitational forces do not act in the plane of motion of the system. This leads to the following expression:

$$V = \frac{1}{2}k_1(\vec{r}_{AB}\cdot\vec{e}_1)^2 + \frac{1}{2}k_2(\vec{r}_{AB}\cdot\vec{e}_2)^2, \tag{B.16}$$

where the elongation of spring i is given by $(\vec{r}_{AB}\cdot\vec{e}_i)$. Assuming isotropic suspension ($k_1 = k_2 = k$) this leads to

$$V = \frac{1}{2}k(x^2 + y^2). \tag{B.17}$$

B.3 Generalised Non-Conservative Forces

Furthermore, the contribution of the non-conservative forces has to be determined. These forces are due to damping and friction. The friction force is assumed to act on each ball in *tangential*

direction, counteracting an increase in β_i, and has a positive value for positive $\dot{\beta}_i$. The generalised non-conservative forces are given by:

$$\underline{Q}^{nc} = \sum_{i=1}^{n_F} \left(\frac{\partial \vec{r}_i}{\partial \underline{q}} \right)^T \cdot \vec{F}_i^{nc} = \left(\frac{\partial \vec{r}_{AB}}{\partial \underline{q}} \right)^T \cdot \vec{F}_{b_1} + \left(\frac{\partial \vec{r}_{AB}}{\partial \underline{q}} \right)^T \cdot \vec{F}_{b_2} + \sum_{i=1}^{2} \left(\frac{\partial \vec{r}_{Bm_i}}{\partial \underline{q}} \right)^T \cdot \vec{F}_{w_i}, \tag{B.18}$$

where $\vec{F}_{b_1}$ and $\vec{F}_{b_2}$ are the damper forces (see figure B.1) and are given by $\vec{F}_{b_i} = -(b_i \dot{\vec{r}}_{AB} \cdot \vec{e}_i)\vec{e}_i$. Once again assuming isotropic suspension yields $b_1 = b_2 = b$. The vectors $\vec{F}_{w_i}$ stand for the friction forces acting on ball i ($i = 1, 2$). The direction in which this friction force acts and the position vector $\vec{r}_{Bm_i}$ is found from figure B.3. One should ensure, however, that both the position

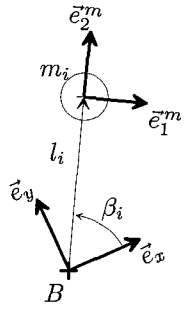

Figure B.3: Friction force acting on ball i.

vector and the force vector corresponding to a generalised non-conservative force are given in the same coordinate system. From figure B.3 it follows that

$$\begin{bmatrix} \vec{e}_1^m \\ \vec{e}_2^m \end{bmatrix} = \begin{bmatrix} \sin\beta_i & -\cos\beta_i \\ \cos\beta_i & \sin\beta_i \end{bmatrix} \begin{bmatrix} \vec{e}_x \\ \vec{e}_y \end{bmatrix}. \tag{B.19}$$

Therefore, the position vector $\vec{r}_{Bm_i}$ and the friction force $\vec{F}_{w_i}$ are

$$\vec{r}_{Bm_i} = l_i \vec{e}_2^m = \begin{bmatrix} l_i \cos\beta_i & l_i \sin\beta_i \end{bmatrix} \begin{bmatrix} \vec{e}_x \\ \vec{e}_y \end{bmatrix}, \text{ and} \tag{B.20}$$

$$\vec{F}_{w_i} = f_{w_i} \vec{e}_1^m = \begin{bmatrix} f_{w_i} \sin\beta_i & -f_{w_i} \cos\beta_i \end{bmatrix} \begin{bmatrix} \vec{e}_x \\ \vec{e}_y \end{bmatrix}, \; i = 1, 2. \tag{B.21}$$

For the total column of generalised non-conservative forces this yields:

$$\underline{Q}^{nc} = \begin{bmatrix} -b(\dot{x} - y\Omega) \\ -b(\dot{y} + x\Omega) \\ -f_{w_1} l_1 \\ -f_{w_2} l_2 \\ 0 \\ 0 \end{bmatrix}. \tag{B.22}$$

This column can be split in two parts: one part containing the damping terms and one part that contains the friction terms:

$$\underline{Q}^{nc} = \underline{Q}^d + \underline{Q}^w = \begin{bmatrix} -b(\dot{x} - y\Omega) \\ -b(\dot{y} + x\Omega) \\ 0 \\ 0 \\ 0 \\ 0 \end{bmatrix} + \begin{bmatrix} 0 \\ 0 \\ -f_{w_1} l_1 \\ -f_{w_2} l_2 \\ 0 \\ 0 \end{bmatrix}. \tag{B.23}$$

This is done because the friction forces depend on the normal forces, which are calculated as constraint forces (see section B.4).

B.4 Constraint Forces

The normal forces acting on each ball are calculated as constraint forces that make sure that the ball stays in contact with the rim of the ABU. These constraints are formulated under the assumption that the distances l_i have a fixed value, namely $l_1 = l_2 = L$. It can easily be seen that this formulates two holonomic, scleronomic constraint equations:

$$\underline{h}(\underline{q}, t) = \underline{0} \quad \Rightarrow \begin{cases} L - l_1 = 0 \\ L - l_2 = 0 \end{cases} . \tag{B.24}$$

These constraint equations are formulated on acceleration level as $\underline{R}\ddot{\underline{q}}_r = \underline{0}$, where $\underline{R} = \underline{h}_{,\underline{q}_r}$:

$$\underline{R}\ddot{\underline{q}}_r = \begin{bmatrix} 0 & 0 & 0 & 0 & -1 & 0 \\ 0 & 0 & 0 & 0 & 0 & -1 \end{bmatrix} \ddot{\underline{q}}_r . \tag{B.25}$$

Using $\underline{R}$, a column of constraint forces is added as an additional term in the equation of motion as $\underline{Q}^{constr} = \underline{R}^T \underline{\lambda}_r$:

$$\underline{Q}^{constr} = \underline{R}^T \underline{\lambda}_r = \begin{bmatrix} 0 \\ 0 \\ 0 \\ 0 \\ -f_{n_1} \\ -f_{n_2} \end{bmatrix} , \tag{B.26}$$

where the normal forces can be found in the column $\underline{\lambda}_r$:

$$\underline{\lambda}_r = \begin{bmatrix} f_{n_1} \\ f_{n_2} \end{bmatrix} . \tag{B.27}$$

The column with non-conservative friction forces, $\underline{Q}^w$ in (B.23), can then be formulated as

$$\underline{Q}^w \in -\underline{S}_r \underline{\lambda}_r, \quad \underline{Q}_w = \begin{bmatrix} 0 \\ 0 \\ -f_{w_1} l_1 \\ -f_{w_2} l_2 \\ 0 \\ 0 \end{bmatrix} . \tag{B.28}$$

Furthermore, the matrix $\underline{S}_r$ can be derived using the Coulomb friction model for the friction forces: $f_{w_i} \in f_{n_i} \mu_i \text{Sign}(\beta_i)$, where Sign denotes the set-valued sign-function (see section 3.1.3).

$$\underline{S}_r = \begin{bmatrix} 0 & 0 \\ 0 & 0 \\ l_1 \mu_i \text{Sign}(\beta_1) & 0 \\ 0 & l_2 \mu_i \text{Sign}(\beta_2) \\ 0 & 0 \\ 0 & 0 \end{bmatrix} . \tag{B.29}$$

B.5 Lagrange's Equations for Systems with Constraints

Lagrange's equations for systems with constraints are given in the following general form:

$$\frac{d}{dt}\left(T_{,\underline{\dot{q}}}\right) - T_{,\underline{q}} + V_{,\underline{q}} = \left(\underline{Q}^{nc}\right)^T + \left(\underline{R}^T \underline{\lambda}\right)^T . \tag{B.30}$$

For the ABU, the following general equation results:

$$\frac{d}{dt}\left(T_{,\underline{\dot{q}}}\right) - T_{,\underline{q}} + V_{,\underline{q}} + \underline{S}_r\underline{\lambda}_r \ni \left(\underline{Q}^d\right)^T + \left(\underline{R}^T\underline{\lambda}_r\right)^T. \tag{B.31}$$

Elaboration of (B.31) yields the following equations of motion for the system:

$$\underline{M}_r(\underline{q}_r)\ddot{\underline{q}}_r - \underline{H}_r(\underline{q}_r, \dot{\underline{q}}_r) + \underline{S}_r\underline{\lambda}_r \ni \underline{R}^T\underline{\lambda}_r, \tag{B.32}$$

where the mass matrix $\underline{M}_r(\underline{q}_r) =$

$$\begin{bmatrix} M & 0 & -m_1 l_1 \sin\beta_1 & -m_2 l_2 \sin\beta_2 & m_1\cos\beta_1 & m_2\cos\beta_2 \\ 0 & M & m_1 l_1\cos\beta_1 & m_2 l_2\cos\beta_2 & m_1\sin\beta_1 & m_2\sin\beta_2 \\ -m_1 l_1\sin\beta_1 & m_1 l_1\cos\beta_1 & m_1 l_1^2 + J_1(\frac{2l_1}{d_1})^2 & 0 & 0 & 0 \\ -m_2 l_2\sin\beta_2 & m_2 l_2\cos\beta_2 & 0 & m_2 l_2^2 + J_2(\frac{2l_2}{d_2})^2 & 0 & 0 \\ m_1\cos\beta_1 & m_1\sin\beta_1 & 0 & 0 & m_1 & 0 \\ m_2\cos\beta_2 & m_2\sin\beta_2 & 0 & 0 & 0 & m_2 \end{bmatrix}, \tag{B.33}$$

and

$$\underline{H}_r(\underline{q}_r, \dot{\underline{q}}_r) = -\left[h_x \quad h_y \quad h_{\beta_1} \quad h_{\beta_2} \quad h_{l_1} \quad h_{l_2}\right]^T, \text{ with:} \tag{B.34}$$

$$\begin{aligned}
h_x &= -2M\dot{y}\Omega - Mx\Omega^2 - m_I e\Omega^2 - \dot{\Omega}(My + m_1 l_1\sin\beta_1 + m_2 l_2\sin\beta_2) \\
&\quad -m_1 l_1(\dot{\beta}_1+\Omega)^2\cos\beta_1 - m_2 l_2(\dot{\beta}_2+\Omega)^2\cos\beta_2 + kx + b(\dot{x} - y\Omega), \\
h_y &= 2M\dot{x}\Omega - My\Omega^2 + \dot{\Omega}(Mx + m_I e + m_1 l_1\cos\beta_1 + m_2 l_2\cos\beta_2) \\
&\quad -m_1 l_1(\dot{\beta}_1+\Omega)^2\sin\beta_1 - m_2 l_2(\dot{\beta}_2+\Omega)^2\sin\beta_2 + ky + b(\dot{y} + x\Omega), \\
h_{\beta_1} &= 2m_1 l_1\dot{x}\Omega\cos\beta_1 + 2m_1 l_1\dot{y}\Omega\sin\beta_1 + m_1 l_1 x\Omega^2\sin\beta_1 - m_1 l_1 y\Omega^2\cos\beta_1 \\
&\quad +\dot{\Omega}(m_1 l_1[x\cos\beta_1 + y\sin\beta_1 + l_1] - \frac{2l_1}{d_1}J_1), \\
h_{\beta_2} &= 2m_2 l_2\dot{x}\Omega\cos\beta_2 + 2m_2 l_2\dot{y}\Omega\sin\beta_2 + m_2 l_2 x\Omega^2\sin\beta_2 - m_2 l_2 y\Omega^2\cos\beta_2 \\
&\quad +\dot{\Omega}(m_2 l_2[x\cos\beta_2 + y\sin\beta_2 + l_2] - \frac{2l_2}{d_2}J_2), \\
h_{l_1} &= 2m_1\dot{x}\Omega\sin\beta_1 - 2m_1\dot{y}\Omega\cos\beta_1 - m_1 x\Omega^2\cos\beta_1 - m_1 y\Omega^2\sin\beta_1 \\
&\quad -m_1 l_1(\dot{\beta}_1+\Omega)^2 + \frac{2J_1}{d_1}\dot{\beta}_1\left(\Omega - \frac{2l_1}{d_1}\dot{\beta}_1\right) + \dot{\Omega}(m_1 x\sin\beta_1 - m_1 y\cos\beta_1), \\
h_{l_2} &= 2m_2\dot{x}\Omega\sin\beta_2 - 2m_2\dot{y}\Omega\cos\beta_2 - m_2 x\Omega^2\cos\beta_2 - m_2 y\Omega^2\sin\beta_2 \\
&\quad -m_2 l_2(\dot{\beta}_2+\Omega)^2 + \frac{2J_2}{d_2}\dot{\beta}_2\left(\Omega - \frac{2l_2}{d_2}\dot{\beta}_2\right) + \dot{\Omega}(m_2 x\sin\beta_2 - m_2 y\cos\beta_2),
\end{aligned}$$

where M is the total mass of the system: $M = M_T + m_I + m_1 + m_2$. Furthermore, $\underline{R}$, $\underline{S}_r$ and $\underline{\lambda}_r$ are given in equations (B.25), (B.29) and (B.27), respectively.

B.6 Non-Dimensional Form of the Equations of Motion

The equations of motion are made non-dimensional by introducing the following non-dimensional coordinates and parameters:

$$\begin{array}{llll}
\bar{x} = \frac{x}{L}, & \bar{l}_1 = \frac{l_1}{L}, & \bar{d}_1 = \frac{d_1}{L}, & \bar{m}_1 = \frac{m_1}{M}, \quad \bar{J}_1 = \frac{J_1}{m_1 d_1^2} = \frac{1}{10}, \\
\bar{y} = \frac{y}{L}, & \bar{l}_2 = \frac{l_2}{L}, & \bar{d}_2 = \frac{d_2}{L}, & \bar{m}_2 = \frac{m_2}{M}, \quad \bar{J}_2 = \frac{J_2}{m_2 d_2^2} = \frac{1}{10}, \\
\bar{\Omega} = \frac{\Omega}{\omega_n}, & \bar{e} = \frac{e}{L}, & \bar{m}_I = \frac{m_I}{M}, & \bar{b} = \frac{b}{2M\omega_n},
\end{array}$$

where $M = M_T + m_I + m_1 + m_2$ and $\omega_n = \sqrt{\frac{k}{M}}$.

Furthermore, a non-dimensional time-scale is introduced: $\bar{t} = \omega_n t$. Consequently, derivatives with respect to the non-dimensional time-scale can be defined:

$$\dot{(\cdot)} = \frac{d(\cdot)}{d\bar{t}} = \frac{1}{\omega_n}\frac{d(\cdot)}{dt} \text{ and } \ddot{(\cdot)} = \frac{d^2(\cdot)}{d\bar{t}^2} = \frac{1}{\omega_n^2}\frac{d^2(\cdot)}{dt^2}.$$

Moreover, non-dimensional versions of the normal (f_{n_i}) and friction forces (f_{w_i}) are introduced:

$$\bar{f}_{n_i} = \frac{f_{n_i}}{m_i\omega_n^2 L}, \text{ and } \bar{f}_{w_i} = \frac{f_{w_i}}{m_i\omega_n^2 L}.$$

Finally, the column of non-dimensional generalised coordinates ($\underline{q}$) can be defined:

$$\underline{q} = \begin{bmatrix}\bar{x} & \bar{y} & \beta_1 & \beta_2 & \bar{l}_1 & \bar{l}_2\end{bmatrix}^T.$$

This leads to the non-dimensional form of the equations of motion:

$$\underline{M}(\underline{q})\ddot{\underline{q}} + \underline{H}(\underline{q},\dot{\underline{q}}) + \underline{S}\,\underline{\lambda} = \underline{R}^T\underline{\lambda}, \tag{B.35}$$

with corresponding new terms (use is made of the fact that $\bar{l}_1 = \bar{l}_2 = 1$):

$$\underline{M}(\underline{q}) = \begin{bmatrix} 1 & 0 & -\bar{m}_1\sin\beta_1 & -\bar{m}_2\sin\beta_2 & \bar{m}_1\cos\beta_1 & \bar{m}_2\cos\beta_2 \\ 0 & 1 & \bar{m}_1\cos\beta_1 & \bar{m}_2\cos\beta_2 & \bar{m}_1\sin\beta_1 & \bar{m}_2\sin\beta_2 \\ -\sin\beta_1 & \cos\beta_1 & 1+4\bar{J}_1 & 0 & 0 & 0 \\ -\sin\beta_2 & \cos\beta_2 & 0 & 1+4\bar{J}_2 & 0 & 0 \\ \cos\beta_1 & \sin\beta_1 & 0 & 0 & 1 & 0 \\ \cos\beta_2 & \sin\beta_2 & 0 & 0 & 0 & 1 \end{bmatrix}, \tag{B.36}$$

$$\underline{H}(\underline{q},\dot{\underline{q}}) = -\begin{bmatrix}h_{\bar{x}} & h_{\bar{y}} & h_{\beta_1} & h_{\beta_2} & h_{\bar{l}_1} & h_{\bar{l}_2}\end{bmatrix}^T, \text{ with:} \tag{B.37}$$

$$\begin{aligned}
h_{\bar{x}} &= -2\dot{\bar{y}}\bar{\Omega} - \bar{x}\bar{\Omega}^2 - \bar{m}_I\bar{e}\bar{\Omega}^2 - \dot{\bar{\Omega}}(\bar{y} + \bar{m}_1\sin\beta_1 + \bar{m}_2\sin\beta_2) \\
&\quad -\bar{m}_1(\dot{\beta}_1 + \bar{\Omega})^2\cos\beta_1 - \bar{m}_2(\dot{\beta}_2 + \bar{\Omega})^2\cos\beta_2 + \bar{x} + 2\bar{b}(\dot{\bar{x}} - \bar{y}\bar{\Omega}), \\
h_{\bar{y}} &= 2\dot{\bar{x}}\bar{\Omega} - \bar{y}\bar{\Omega}^2 + \dot{\bar{\Omega}}(\bar{x} + \bar{m}_I\bar{e} + \bar{m}_1\cos\beta_1 + \bar{m}_2\cos\beta_2) \\
&\quad -\bar{m}_1(\dot{\beta}_1 + \bar{\Omega})^2\sin\beta_1 - \bar{m}_2(\dot{\beta}_2 + \bar{\Omega})^2\sin\beta_2 + \bar{y} + 2\bar{b}(\dot{\bar{y}} + \bar{x}\bar{\Omega}), \\
h_{\beta_1} &= 2\dot{\bar{x}}\bar{\Omega}\cos\beta_1 + 2\dot{\bar{y}}\bar{\Omega}\sin\beta_1 + \bar{x}\bar{\Omega}^2\sin\beta_1 - \bar{y}\bar{\Omega}^2\cos\beta_1 \\
&\quad +\dot{\bar{\Omega}}(\bar{x}\cos\beta_1 + \bar{y}\sin\beta_1 + 1 - 2\bar{d}_1\bar{J}_1), \\
h_{\beta_2} &= 2\dot{\bar{x}}\bar{\Omega}\cos\beta_2 + 2\dot{\bar{y}}\bar{\Omega}\sin\beta_2 + \bar{x}\bar{\Omega}^2\sin\beta_2 - \bar{y}\bar{\Omega}^2\cos\beta_2 \\
&\quad +\dot{\bar{\Omega}}(\bar{x}\cos\beta_2 + \bar{y}\sin\beta_2 + 1 - 2\bar{d}_2\bar{J}_2), \\
h_{\bar{l}_1} &= 2\dot{\bar{x}}\bar{\Omega}\sin\beta_1 - 2\dot{\bar{y}}\bar{\Omega}\cos\beta_1 - \bar{x}\bar{\Omega}^2\cos\beta_1 - \bar{y}\bar{\Omega}^2\sin\beta_1 \\
&\quad -(\dot{\beta}_1 + \bar{\Omega})^2 + 2\bar{J}_1\dot{\beta}_1(\bar{d}_1\bar{\Omega} - 2\dot{\beta}_1) + \dot{\bar{\Omega}}(\bar{x}\sin\beta_1 - \bar{y}\cos\beta_1), \\
h_{\bar{l}_2} &= 2\dot{\bar{x}}\bar{\Omega}\sin\beta_2 - 2\dot{\bar{y}}\bar{\Omega}\cos\beta_2 - \bar{x}\bar{\Omega}^2\cos\beta_2 - \bar{y}\bar{\Omega}^2\sin\beta_2 \\
&\quad -(\dot{\beta}_2 + \bar{\Omega})^2 + 2\bar{J}_2\dot{\beta}_2(\bar{d}_2\bar{\Omega} - 2\dot{\beta}_2) + \dot{\bar{\Omega}}(\bar{x}\sin\beta_2 - \bar{y}\cos\beta_2),
\end{aligned}$$

$$\underline{R} = \begin{bmatrix}0 & 0 & 0 & 0 & -1 & 0 \\ 0 & 0 & 0 & 0 & 0 & -1\end{bmatrix}, \tag{B.38}$$

$$\underline{S} = \begin{bmatrix} 0 & 0 \\ 0 & 0 \\ \mu_1\text{Sign}(\dot{\beta}_1) & 0 \\ 0 & \mu_2\text{Sign}(\dot{\beta}_2) \\ 0 & 0 \\ 0 & 0 \end{bmatrix}, \tag{B.39}$$

$$\underline{\lambda} = \begin{bmatrix}\bar{f}_{n,1} \\ \bar{f}_{n,2}\end{bmatrix}. \tag{B.40}$$

Appendix C

Derivation of the Equations of Motion of the Motor

C.1 General Equation of Motion

As was already mentioned in section 3.2, a second-order differential equation is used to describe the dynamics of the motor driving the ABU. In figure C.1, a schematic representation of the ABU is given. It is assumed that the ABU and CD are fixed rigidly to the shaft of the motor. In

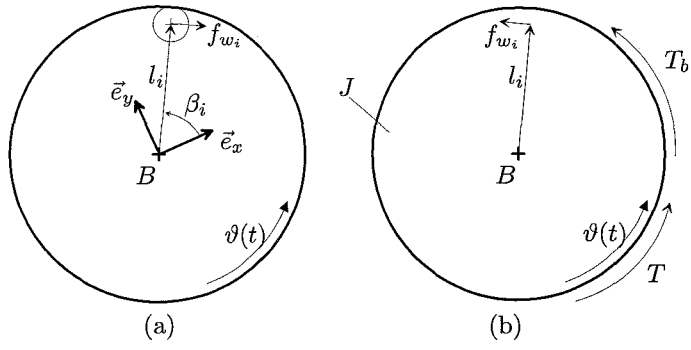

Figure C.1: Force exerted on the ball (a) and forces/moments acting on CD (b).

figure C.1(b), J represents the moment of inertia of the ABU, CD and imbalance around point B. T represents the torque from the motor and is considered as a control input here. Furthermore, T_b is the friction couple acting on the motor (for example due to friction in the bearings) and a reaction force from the friction on ball i is present on radius l_i $(i = 1, 2)$, see figure C.1(a). The second-order differential equation describing the system in figure C.1(b), is the following:

$$J\ddot{\vartheta} = T + T_b + \sum_{i=1}^{2} f_{w_i} l_i. \tag{C.1}$$

Note the direction of the friction couple T_b and the friction forces f_{w_i} $(i = 1, 2)$. Both the friction couple T_b and the friction forces act in the same direction as the rotation ϑ. In the experimental setup the direction of ϑ is reversed (clockwise direction), so the friction couple and the friction forces counteract the rotation of the ABU, as they are assumed to do.

C.2 The Controller

In the documentation of the motor control (see [Phi02]), it is stated that the angular velocity controller is a PI-controller (proportional and integral control action) on the angular velocity. The control input hence is given by equation (C.2):

$$T = Ke + I\int e, \tag{C.2}$$

where

$$e = \dot{\vartheta}_{ref} - \dot{\vartheta}. \tag{C.3}$$

From the derivation of the equation of motion of the ABU it is known that $\vartheta = \int_0^t \Omega(\tau)d\tau + \vartheta(0)$ ($\vartheta(0)$ is assumed to be zero). Therefore $\int e = \vartheta_{ref} - \theta + e(0)$ and the total control input becomes:

$$T = K(\dot{\vartheta}_{ref} - \dot{\vartheta}) + I(\vartheta_{ref} - \vartheta). \tag{C.4}$$

The initial value of the integrator action $e(0)$ is also assumed to be zero.

C.3 The Resulting Equation of Motion

Combining equation (C.1) and (C.4) yields the total equation of motion for the motor driving the ABU:

$$J\ddot{\vartheta} - K(\dot{\vartheta}_{ref} - \dot{\vartheta}) - I(\vartheta_{ref} - \vartheta) = T_b + \sum_{i=1}^{2} f_{w_i} l_i. \tag{C.5}$$

For sake of convenience and parameter identification this is written as

$$J[\ddot{\vartheta} - 2\xi\omega_m(\dot{\vartheta}_{ref} - \dot{\vartheta}) - \omega_m^2(\vartheta_{ref} - \vartheta)] = T_b + \sum_{i=1}^{2} f_{w_i} l_i, \tag{C.6}$$

where ω_m and xi denote the natural frequency in rad/s and the non-dimensional damping coefficient of the motor system, respectively.